Extreme precipitation events over southern India during the year 2015- Curious interactions of El Nino, MJO, and associated waves.

Rakesh Teja Konduru[1, 2] and Mrudula G[1]

[1]*Department of Geography, Tokyo Metropolitan University, Tokyo, Japan.*

[2]*Centre for Electromagnetics (CEM), Council of Scientific and Industrial Research (CSIR), National Aerospace Laboratories (NAL), Kodihalli, Bengaluru, India - 560017.*

Submitted to

Corresponding author email:- rakeshtejak@gmail.com

Abstract

The cause of extreme precipitation events, which deadly flooded Tamil Nadu state of southern India during the northeast monsoon season of 2015 was investigated, and the results were presented in this paper. Though a strong El Nino prevailed during the events, the effect of El Nino is suppressed by the tropical variabilities in the Indian Ocean. A power spectrum analysis was performed to find out the kind of tropical variabilities in NCEP variables like wind fields, Omega, precipitation rate, and soil moisture at 0-10 cm. The spectrum analysis resulted in significant periodicities of 30-40 days and 7-20 days during the extreme events over southern India. Those frequencies were linked with the convectively coupled equatorial waves (CCEWs) like Madden-Julian Oscillations (MJO), and, it was found that the cause of El Nino's suppression is a manifestation of the CCEWs. The dynamical mechanism behind those interactions was investigated to know the specific connections of two major tropical variabilities El Nino and MJO. Further exploration was done by performing composite analysis of extreme precipitation events during historical El Nino (moderate to very strong) and MJO (active phases over the Indian Ocean) events from 1997-2014 to know the possible interaction between El Nino and MJO. The composite analysis contributed an insight into the interactions of El Nino and MJO. This analysis concludes a hypothesis, which states that if a prevailing, moderate to very strong El Nino as a background low-frequency wave superimposed with high-frequency wave like active MJO in the equatorial Indian Ocean during October-December season, then blended El Nino & MJO wave suppresses the effect of background prevalent El Nino. Such a clampdown of El Nino by blended El Nino & MJO wave roots the cause of extreme precipitation over the southeastern India. This study reveals a new dimension to the El Nino and MJO interactions in intraseasonal

time scale, which could be exploited in the prediction of extreme precipitation events during northeast monsoon season.

Keywords

El Nino, Madden-Julian Oscillations, Northeast Monsoon, convectively coupled equatorial waves, Extreme precipitation, subtropical westerlies, and subtropical highs.

1. Introduction

Northeast monsoon (hereafter NEM; October-December, OND; it is also known as retreating monsoon or winter monsoon; Dhar et al., 1983; Zubair, 2002) season is the main cultivation season of states like Tamil Nadu, southern Andhra Pradesh in the South India and also of Sri Lanka. In this season, all India receives 11 % of annual rainfall, and South India receives up to 30%-60% of the annual precipitation. Apart from the Indian region, the Sri Lankan region also receives up to 50% of annual rainfall. Also, the southeastern India receives the maximum amount of rainfall during the same season and rain decreases further inland. Rajeevan et al. (2012) studied the variability of the OND seasonal rains, and they found it to be 25 %, which is more than Indian summer monsoon rainfall variability (10%). Therefore, it is crucial in predicting the NEM precipitation variability. Yadav R. K. (2011) had shown the substantial variability of NEM rainfall in recent years. The extreme precipitation events in 2015 exemplify one such variability in NEM rainfall over the eastern coast of Tamil Nadu state in India. Those extreme precipitation events occurred during three different periods, i.e. November 9 to 10, November 15 to 16 and November 30 to December 2 (hereafter these events are referred as case-1, case-2, and case-3 respectively). These extreme events resulted in severe flooding, consumed numerous deaths, and loss of properties in southeastern India, especially, the Chennai that is totally inundated in floods. The World Meteorological Organization (WMO), India Meteorological Department (IMD), and Regional Integrated Multi-Hazard Early Warning System for Africa and Asia (RIMES) released their predictions in October 2015 that the strong El Nino conditions might affect the NEM rainfall. However, their predictions could not clearly address the potential impact region over southern India and Sri Lanka, and, they also stated that the cause of such extreme events during NEM of southern India has been unresolved, and the

exact root of its origin requires proper investigation. The current paper investigates the ultimate cause of those extreme events.

1.1 Background

The fundamental variability of NEM rainfall is linked to ocean-atmosphere coupled phenomenon like El Nino/Southern Oscillation (ENSO; Ropelewski and Halpert, 1987, 1989). Most of the earlier studies had pointed out the linkage as inter-annual variability of NEM rainfall with El Nino/Southern Oscillation (propagates in the background of the global weather as a low-frequency wave); and their relationship supplemented by the presence of strong easterlies at 850 mb over the equatorial Indian Ocean and low-level moisture convergence. Suppiah (1997) has studied the relationship between ENSO and NEM by compositing the extreme rainfall events and found positive anomalies of NEM rainfall over southern India during El Nino years. Recent studies showed that the relationship between ENSO and NEM had been strengthening over South Asia (Zubin et al., 2006; Pankaj Kumar et al., 2007). Yadav R. K. (2011) has studied the decadal relationship between ENSO and Inter-annual variability (IAV) of NEM rainfall. They quoted that in El Nino years, NEM rainfall is either normal or above normal, which is also shown by Rajeevan et al. (2012).

Few studies depicted the intra-seasonal variability (ISV) of NEM rainfall. Nageswara Rao G. (1999) has reviewed the intra-seasonal relationship of NEM rainfall with Southern Oscillation (SO) over South India, which explained the occurrence of peak rainfall over the same region. Apart from it, northward propagation of organized convection and the presence of 20-60 day oscillation in NEM (Charlotte B. V. et al., 2012) are some of the features of ISV. Another major global intra-seasonal pattern, which affects NEM rainfall is the Madden-Julian Oscillation

(MJO; Madden et al., 1971; Zhang, 2005). The MJO is one of the important tropical variability associated with organized convection. Jia X et al. (2011), has shown the influence of MJO on the northward transport of the moisture from the Indian Ocean and the Bay of Bengal during NEM. Apart from above ISV of NEM rainfall, other tropical variabilities like equatorial waves that propagate along the equator at different time scales (Wheeler et al., 1999). Those waves called as convectively coupled equatorial waves (CCEW). Some of the identified CCEW are Kelvin waves, equatorial Rossby waves, mixed Rossby & Gravity waves and Madden-Julian Oscillation. The active phase of MJO especially is an enhanced zone of convection with co-existence of CCEWs like equatorial trapped Kelvin waves and equatorial Rossby waves (Majda et al., 2004; Mapes et al., 2006). In general, Kelvin waves are the most prominent source for synoptic scale tropical rainfall variability, which travel through MJO (B Wang, 2002). There have been very fewer studies done related to the impact of individual CCEWs, and CCEWs co-existence with MJO on NEM rainfall. However, the interactions of MJO & Kelvin waves and interactions of MJO & equatorial waves are well documented in individual works of Roundy, 2007; Hendon et al., 1994; Guo et al., 2014. Furthermore, those interactions are fundamentally perceived in the experiment Year of Tropical Convection (YOTC; Gottschalck et al., 2010).

It is necessary to fill the gap of knowledge on the influence of individual CCEWs, and blended CCEWs with MJO, on NEM rainfall. Apart from the El Nino & MJO interactions, its impact on NEM is also imperative because they are the dominant modes of tropical variabilities. Hendon et al. (2007) have observed the seasonal dependence of El Nino and MJO over the equatorial Pacific Ocean. Current study outlines the interactions of El Nino and MJO, and, its exact role in triggering the extreme events in 2015 over southeastern India during winter monsoon.

2. Data and methodology

2.1 Observational and reanalysis data

The datasets employed in the analysis are 1) Tropical Rainfall Measuring Mission (TRMM) 3B42 real time (RT) v7 0.25^o precipitation rate (mm/day). TRMM 3B42 RT is a combination of TRMM 3B40RT high-quality precipitation estimate (different satellites like TRMM calibrated TMI, AMSR-E, SSMI, AMSU, and MHS) and 3B41RT variable rain rate infrared precipitation estimate from geostationary infrared observations. 2) Daily merged multi-satellite-gauge real-time rainfall (mm/day) 0.25^o resolution dataset for Indian region is considered (Mitra et al., 2003, 2009, and 2013b). In this rainfall product, Global Precipitation Measurement (GPM; Hou et al., 2014*)* project multi-satellite rainfall estimates are merged with the IMD gauge data over Indian region. Satya Prakash et al. (2015) has studied accurateness in the detection of heavy rain events by using TRMM and GPM rainfall datasets, which became our motive to show the three extreme precipitation events by using that space-borne rainfall observation. 3) Global Precipitation Climatology Product (GPCP) v1.2 1.0^o daily precipitation rate (mm/day) is also utilized (Huffman et al., 2001). 4) India Meteorological Department (IMD) 0.5^o daily rainfall (mm/day) is acquired to select the moderate to heavy rain events over Indian region (Mitra et al., 2009). Moreover, 5) National Center for Environmental Research Prediction - National Center for Atmospheric Research (NCEP-NCAR) reanalysis-1, (Kalnay et al., 1996) 6 hourly 2.5^o data set is obtained to analyze the dynamic atmosphere conditions during the events. From the NCEP reanalysis, variables like wind fields, Omega, relative humidity up to 17 pressure levels, and surface variables like sea level pressure, soil moisture at 0-10 cm, and lifted index were chosen. Apart from above variables, precipitation rate of NCEP-NCAR reanalysis-1 in a Gaussian grid of T64 is also exploited in the analysis.

2.2 Methodology

Anomalies of selected variables from NCEP-NCAR reanalysis-1 dataset were calculated for the period 1981-2015 based on the 1981-2010 climatology. A composite of the 2015 winter monsoon extreme precipitation cases were created by using anomalies over the region 10^0S – 40^0N & 40^0E – 120^0E (it covers entire Indian region and neighboring oceans; that region was named as domain-1). The power spectrum analyses of the composites of each case were performed to know the dominant modes of periodicities during NEM over the area 8^0N–20^0N & 75^0E–85^0E (the region was named as domain-2). Domain-2 cover only land fractions of southern India, which was also named as NEM region because winter monsoon rainfall is received in most of the parts of that region. From the composites, mean was removed, detrended, and tapered before passing through Fast Fourier Transform (FFT). These preprocessing steps minimize the chances of ringing and leakage. Subsequently, those periodicities were employed to extract convectively coupled equatorial waves over 5^0 S – 5^0 N (CCEWs) by using a band-pass filter for each wave separately over each grid point. Some of the CCEWs like Kelvin waves were obtained from band-pass filtering of the variables for wavenumber 1 to 14 as done by Wheeler et al. (1999) and Straub et al. (2002). The equatorial Rossby waves were filtered in a similar manner, but for wavenumber -10 to -1 as quoted by Kiladis et al. (2009). All of the variables were initially detrended and then tapered in time and filtering was done with a specific wavenumber of the individual CCEWs by using discrete Fourier transform on the periodic data. The MJO wave was extracted by applying a band-pass filter for wavenumbers 1 to 5 as mentioned in Wheeler et al. (1999) over a time window 30-90 days.

Another composite analysis of historical extreme rainfall events from 1981-2014 and 1997-2014 (table-1) was carried out over southern India during OND season. The rain events

were clustered based on the criteria used by Pattanaik et al. (2010) and Guhathakurta et al. (2011) into heavy and extreme rainfall events if daily rainfall is more than 64.5 mm in domain-2. The extreme rain events were separated prudently into El Nino and Normal events (Normal events do not include El Nino and La Nina year events) by using the Oceanic Nino Index (ONI). The ONI is defined as three months running mean of sea surface temperature anomalies in the region Nino 3.4 (5^oS- 5^oN & 120^oW-170^oW). The El Nino is further classified as moderate if ONI is 1.0 to 1.4, strong El Nino if ONI is 1.5 to 1.9) and very strong El Nino if ONI is more than or equal to 2.0. Those El Nino and Normal extreme rainfall events were further categorized into active MJO (active phases 2 and 3 of MJO) and weak MJO events over the Indian Ocean region by using Real-time Multivariate MJO RMM1 and RMM2 index. The Real-time Multivariate MJO Index is obtained by projecting daily anomalies of 850 mb zonal wind, 200 mb zonal wind, and outgoing longwave radiation onto the multiple-variable EOFs (Wheeler et al., 2004). The MJO was considered strong if the index magnitude is more than one. Otherwise, it is hard to discern weak MJO signal in the considered meteorological variables. Thus, categorized extreme rainfall events were grouped into different composites like Normal, El Nino, MJO, and El Nino & MJO. Further, the difference among those composites was calculated and analyzed to understand the interactions of El Nino & MJO, El Nino & Normal, Normal & MJO, El Nino & MJO with MJO, and El Nino & MJO with El Nino during extreme events in OND season. The differences of composites were validated with the Student's t-test, which ensures the robustness of residuals, and to see whether the composite states significantly differs from the base state; and only more than 95 % significant part was showed in the difference composites.

3. Results and Discussions

188 During OND season of 2015, the southeastern India witnessed extreme rainfall events
189 during three different periods, i.e. November 9 to 10 (case-1), November 15 to 16 (case-2) and
190 November 30 to December 2 (case-3), which caused flooding in the southeastern parts of Tamil
191 Nadu state in India.

192 ***3.1 Synoptic Observations***

193 Composites of GPM and TRMM rainfall were created in case-1, case-2, and case-3. The
194 rainfall is widespread over southeastern India in both case-1 (fig 1 a1) and case-2 (fig 1 b1),
195 whereas, in case-3 (fig 1 c1) rainfall is localized in nature over Chennai. All of these events lead
196 to heavy floods in Chennai and its neighborhoods, which will be the region of focus in the
197 current section. In case-1 (fig 1 a2), the negative anomalies of sea level pressure over southern
198 India represent the formation of a low-pressure area (LPA) in the south Bay of Bengal (hereafter
199 BOB). Subsequently, it strengthened to a deep depression in the south BOB and moved
200 northwestward over to land after crossing the southeastern coast at Pondicherry. Similarly, case-
201 2 (fig 1 b2) is an LPA with cyclonic circulation laid at 1000 mb, in southern BOB. At the same
202 time, to the south of LPA below the equator, two cyclonic circulations are noticed at 1000 mb
203 and 850 mb. However, an upper air cyclonic circulation (UAC) is observed in case-3 (fig 1 c2)
204 over southeastern India. The noteworthy point is that the source of moisture to all of these cases
205 is southerlies from the equatorial Indian Ocean (shown in the lower panel of figure 1). However,
206 the sinks of moisture are different kinds of mesoscale convective systems formed near the
207 southeastern coast of India.

208 Figure 2 demonstrates the time series of a vertical cross-section of meteorological
209 variables averaged over 12^{o}N-13^{o}N & 80^{o}E over Chennai and its neighborhoods. Very strong

updrafts (fig 2c, Omega) from surface to 200 mb, with strong positive relative humidity anomalies from 850 mb to 500 mb (fig 2e), sufficient negative lifted index anomalies (fig 2b, red line), and adequate fall in sea level pressure (fig 2b, green line) helped the mesoscale convective system in case-1 to develop further from low pressure area to deep depression. The presence of very less wind shear (fig 2d) supported the deep depression to sustain without being dispersed and resulted with a peak precipitation of ~70 mm/day (fig 2a). However, in case-2, the weather conditions are similar to case-1 but low in magnitude, resulted in the development of mesoscale convective system related to well-marked low. Along with those weather conditions, the lifted index (fig 2b) maintained the meteorological instability to support the cyclonic circulation by moisture convergence and resulted in peak precipitation of 50 mm/day (fig 2a). Interestingly, in Case-3, though there was an enormous amount of relative humidity (fig 2e), it did not contribute much rain due to weak updrafts (fig 2c) and high wind shear (fig 2d). Therefore, case-3 event did not show much rainfall as compared to case-1 & case-2, but the rainfall received is around 30 mm/day (fig 2a). The rainfall in case-1 clearly represents extreme precipitation event and in case-2 & case-3 as rather heavy rain events based on the criteria used by Pattanaik et al. (2010), and Guhathakurta et al. (2011).

3.2 NCEP anomalies and overview of wind fields

Composites of NCEP zonal wind anomalies were created for three cases. In case-1, cyclonic circulation associated with a deep depression formed at 1000 mb (fig 1a) laid over southern India extends up to 500 mb (fig 3d left column). A positive velocity potential at 850 mb over South India and BOB represents the presence of converging winds (fig 3g; green color contour). At 500 mb positive velocity potential (fig 3d) seems to shift eastward, and a zone of negative velocity potential appears over the western coast of southern India. However, the

cyclonic circulation at 200 mb vanishes due to diverging winds represented by negative velocity potential (fig 3a; magenta color contour). While in case-2, over southern India, cyclonic circulation extends from 1000 to 500 mb (fig 3e), and a positive velocity potential shows the presence of converging winds at these levels. The cyclonic circulation at 200 mb disappears due to diverging winds (fig 3b), which is demonstrated by negative velocity potential. Nevertheless, in case-3, UAC is weak in nature at 850 mb (fig 3i), but it is strong at 500 mb (fig 3f) that covers entire southern India and represented by positive velocity potential at those levels. The presence of diverging winds represented by negative velocity potential at 200 mb (fig 3c) terminates the circulation at this level. The similarity in these three cases is the presence of westerlies that dominated over the North Indian Ocean around 80^{o}E at 850 mb & 500 mb, but these westerlies are found to be weak in case-1.

The motivating point is that all of the three cases have shown southerly wind anomalies at 850 mb (fig 4g-h-i) and 500 mb (fig 4d-e-f). In case-2 and case-3, southerly wind anomalies are strong as compared to case-1. The presence of an active zone of positive relative humidity anomalies (green color contour) over southern India and southerly winds clearly portrays the manner by which these winds bring moisture from the Indian Ocean (source) and moves further north through southern India. Consequently, the mesoscale convective systems developed over south India act as a sink of moisture and southerly winds serve as a carrier for it. In general, during NEM over southern India, northeasterly winds prevail (Dhar et al., 1983), and they act as a carrier of moisture from the source BOB. However, these three cases are different in concerning both the origin and transport of moisture over southern India.

3.3 Vertical cross-sections of dynamical parameters

Figure 5 shows the longitudinal and latitudinal vertical cross-sections of Omega and relative humidity anomalies. The figure 5a & 5b represents mean of OND season of 2015 and figure 5c & 5d shows mean for the period November 8 to 16, 2015, which consists of case-1 & case-2 events. These two events are observed to be similar regarding meteorological conditions as explained in previous sections. The left, and right panels in figure 5 describe Omega anomalies scaled by zonal wind anomalies and meridional wind anomalies respectively. Moreover, the shaded portion in the figure 5a & 5c illustrates relative humidity anomalies averaged over 5^{o}S–5^{o}N. The presence of strong positive relative humidity anomalies and strong updrafts over the Pacific Ocean conveys about the shift in the Walker circulation to the east (fig 5a), which in general happens during climatic variability like El Nino as explained by Philander (1990). Besides, over maritime continent subsidence of dry air is clearly observed. An interesting feature of strong updrafts until 600 mb is perceived over 80^{o}E with sufficient positive anomalies of relative humidity. Figure 5c is a mean of variables as mentioned above from November 8 to 16 (which includes extreme and rather heavy rain events of OND season 2015). It is similar to the fig 5a, except very strong updrafts over the Pacific Ocean and around 80^{o}E in the Indian Ocean. The presence of strong updrafts and substantially high relative humidity until 500 mb level supports the anomalous convergence of moisture.

Figure 5b & 5d shows vertical cross-sections along latitude 40^{o}S–40^{o}N averaged over 75^{o}E–85^{o}E. The updrafts over equator are weak as seen in figure 5b. However, updrafts over 30^{o}N and 30^{o}S are seen from lower troposphere to upper troposphere and at mid-troposphere respectively. Over 10^{o}N-15^{o}N, subsidence of dry air is witnessed. The figure 5d is a mean from November 8 to 17, 2015, in which stout updrafts and very high moisture are seen until 500 mb around 10^{o}N-15^{o}N. As a result, these anomalous circulations of moisture affect the southern part

of India that comes in 10°N-15°N. In addition to it, significant moisture convergence is observed around 30°S & 30°N. These latitudinal and longitudinal cross-sections exhibit strong updrafts due to convergence and transport of moisture around 80°E from the north Indian Ocean to 10°N - 15°N & 75°E–85°E region of India.

These results imply the solid connections between sink & source regions of wind fields and humidity to the large-scale tropical variabilities. Unfortunately, there was no such direct link found with tropical variabilities like El Nino. In general, during El Nino, the source of moisture is same as observed in current cases, but the carrier is easterlies over Northern Indian Ocean. These easterly winds are not seen during the current events. Moreover, no such profitable link observed between NEMR with IOD due to neutral Indian Ocean Dipole (IOD) conditions during 2015 NEM because only during positive IOD phase southerlies and the Indian Ocean acts as a carrier and source of moisture respectively. Thus, the source and carrier of moisture created a curiosity to know about the exact linkage of moisture transport during the current cases with the kind of tropical variability.

3.4 The dominant periodicities of ISV over NEM region.

Power spectrum analysis is performed over nine meteorological parameters. These parameters include, precipitation rate (both TRMM 3B42 and NCEP reanalysis), mid-tropospheric temperature (MTT; 500 mb), mid-tropospheric humidity (MTH; 500 mb), zonal wind at 925 mb & 200 mb, meridional wind at 925 mb & 200 mb, and soil moisture at 0-10 cm (fig 6). Accordingly, dominant periodicities of these parameters are obtained over NEM region (8°N - 20°N & 75°E - 85°E; OND). The analysis suggests that few of the parameters like upper tropospheric humidity (fig 6d), Zonal wind at 200 mb (fig 6f) and soil moisture at 0-10 cm (fig

6i) showed periodicities of 30-40 days with 90% significance, whereas Zonal wind at 200 mb displayed similar variability with 80% significance. The soil moisture is analyzed to diagnose whether a built-in memory of soil moisture, which is about weeks to two months or much longer than that of atmospheric variables (Vinnikov et al., 1991; 1996; Entin et al., 2000), plays any role in retaining the periodicity of the tropical variability. Encouragingly, soil moisture spectrum very clearly exhibits the ability of it to store the 30-40 days oscillation. Also, MTH also exhibited 30-40 variability in the tropical atmosphere (e.g., Mote et al., 2000; Tian et al., 2006). Whereas, the 30-40 day periodicity is barely significant in MTT (fig 6c), zonal wind 925 mb (fig 6e), and precipitation rate (fig 6a & 6b; TRMM & NCEP). Moreover, 7-20 day periodicity is also observed with 90 % significance in almost all parameters. This analysis brings out an idea of the presence of 30-40 days and 7-20 oscillation during OND of 2015.

The presence of 7-20 days oscillation in the power spectrum analysis, along with that the features suchlike anomalous westerlies near to the equator in three extreme event cases at 850 mb (fig 3) resemble them like Kelvin wave as described by Thomson, W. (1989). The twin cyclonic circulations across the equator over the southern Indian Ocean in case-1 & case-2 corresponds to equatorial Rossby waves with 9-72 day oscillation as described by G. N. Kiladis et al. (1996) respectively. These notable waves propagate to the east and west respectively. On the other hand, at 850 mb the meridional wind anomalies show (fig 4) northward propagation during case-2 & case-3. That signifies the observed westerly anomalies near to the equator are not only Kelvin waves by its own, but accompanied by a particular kind of oscillations like Madden-Julian Oscillations (30-90 days; MJO). These observations show that the extreme rainfall events could be due to MJO, equatorial Rossby waves, and Kelvin waves, which are also known as convective coupled equatorial waves (CCEWs).

3.5 Convectively Coupled Equatorial Waves (CCEW)

NCEP anomalies of the wind field, velocity potential, sea level pressure, and precipitation rate anomalies are employed to extract the corresponding CCEW for the events as described in section 2.2. The above meteorological variables were passed through 30-90 days band-pass filter, which filtered out only those unusual patterns that have the same period as of the MJO (fig 7; In this section only filtered variables were analyzed). It is evident that in most of the cases, westerly wind anomalies are dominated near to the equator, and two cyclonic circulations appear across the equator at 850 mb, which is associated with the MJO (Wheeler et al., 1999). In case-1, the well-marked negative anomalies of sea level pressure (magenta color dashed line at 1000 mb) over southern India are associated with cyclonic circulation formed due to the deep depression at 1000 mb (fig 7d). Apparently, that could be a region of the enhanced organized convection of MJO over southern India, which is indicated by positive velocity potential (green color contour). The convectively coupled enhanced convective region of the MJO could be identified as Kelvin wave, which is reported in the works of Nakazawa (1988), Takayabu et al. (1991), Dunkerton et al. (1995), and Straub et al. (2002). These Kelvin waves propagate eastward as reflected from the high westerly wind anomalies at 850 mb in the Indian Ocean. At higher levels like 200 mb, filtered negative velocity potential anomaly (blue dash line) depicts diverging wind fields with easterly zonal wind anomalies (fig 7a).

However, in case-2, the presence of negative sea level pressure anomalies to both sides of the equator beckoned it as an equatorial Rossby wave which propagates westwards (fig 7e).This observation is in agreement with the results obtained by Kiladis et al. (1995), Wheeler et al.

(2000), and Roundy et al. (2004b). A very active zone of westerly wind anomalies shifted to northwards around 80^{o}E demonstrating the presence of Kelvin wave, which is a major component of MJO for enhanced convection that propagates eastward. Together with above CCEWs, interestingly, in case-2, all of the dominant modes of equatorial variability are observed at the same region. This co-existence of CCEWs could be attributed to the substantial enhancement of the westerly winds over the same area, which is evident from the wind field observations in the figure 7e. This kind of co-existence of dominant modes of CCEWs like MJO, Kelvin wave, and equatorial Rossby wave immensely contributed to the mesoscale convective systems development over the southern India. The similar results related to the co-existence of CCEWs are also observed in the work of Roundy et al. (2010). The co-existence of CCEWs around 80^{o} E could prolong the convective activities over the same region. Such a prolonged convective activity due to the co-existence of CCEWs is also reported by Roundy (2007). In case-3, negative sea level pressure anomalies over the Indian Ocean (at surface magenta color dashed line) correspond to the synoptic system developed over that region, which is represented by a positive velocity potential (fig 7f). However, the twin cyclonic circulations across the equator in 850 mb zonal wind anomaly show the presence of equatorial Rossby waves. The westerly wind anomalies at 850 mb are close to the equator and are not as strong as seen in case-2. One of the peculiar features of case-3 is the existence of anomalous trough in westerlies at 200 mb (fig 7c), which are not regarded in case-1 and case-2 that are dominated by subtropical highs. This anomalous trough in westerlies separates the case-3 from remaining cases upper tropospheric zonal wind anomalies. It clearly implies that along with MJO some other phenomenon might have existed during case-3, which modulated the subtropical westerlies to form a low trough and pushed the lower level westerlies towards the equator.

The striking point is that the enhanced convection of the MJO has contributed to the case-1, case-2, and case-3 rainfall events with different convectively active modes. Figure 8 illustrates the filtered convectively active modes of CCEWs. Figure 8a shows the MJO, and equatorial Rossby waves in filtered 850 mb, 200 mb zonal winds, and precipitation rate, which supported in the formation of a tropical depression over the southern Indian Ocean that caused extreme rain over southeastern India in case-1. A similar kind of CCEWs existed in case-3, which influenced the mesoscale convective system over southeastern India (fig 8c). However, case-2 is a combination of different kinds of CCEW like Kelvin waves and equatorial Rossby waves within MJO and contributed to widespread rain over southeastern India (fig 8b). This analysis confirms the influence of CCEWs on different mesoscale convective systems, which caused extreme events over southeastern India.

Another crucial thing is that though CCEWs has affected the weather over southeastern India, its strong influence even in the presence of very strong El Nino in the background is uncommon. Since 2015 is reported as a year of very strong El Nino, it is not apparent to have such a kind of dominated westerlies near the equator, which could suppress the impact of easterlies associated with El Nino lower tropospheric levels over the Indian Ocean region. Generally, in the past, during very strong El Nino years of 1982 & 1997 in OND season, all of the extreme rainfall events are accompanied with easterly wind anomalies at 850 mb, and there were no traces of suppression of easterly winds associated with El Nino by westerly winds associated with the MJO. Therefore, it is crucial to know the interactions between MJO and El Nino, and the mechanism of it, which caused extreme precipitation events. For this analysis, case-2 event is selected out of three cases to explore the interaction between the MJO and El

Nino because in case-2, Kelvin and equatorial Rossby waves co-existed within MJO, and it is assumed as an ideal condition.

3.6 Interactions between El Nino and MJO

The extreme events (precipitation more than 64.5 mm/day) from 1997-2014 were composited as Normal, MJO, El Nino, and El Nino & MJO (hereafter these composites are called as NC, MC, EC, and EMC respectively) during OND season. Here, EMC events were those cases in which El Nino and MJO exist together. These composites were assumed as waves and interactions among those composites were investigated. Here, Normal composite wave does not to include El Nino, La Nina and active MJO events of phase 2 & 3. The list of extreme rainfall events used in the composites was presented in table-1, and the procedure for selecting composites was already discussed in section 2.2. These composites were prepared (table-2) by using NCEP zonal winds (850 mb, 200 mb), and precipitation rate anomalies (NCEP and GPCP; TRMM was not considered because it does not include 1997 very intense El Nino).

Figure 9 illustrates a difference between the different combinations of composite waves (it is called as the residual), like, EC & NC, EC & MC, EMC & NC, EMC & MC, MC & NC, and EMC & EC, which are denoted as A, B, C, D, E and F residuals respectively. These residuals exemplify all of those remnant waves, which are dominant during the past extreme events in OND season. Persuasive results are noticed from residuals in the zonal wind anomalies (upper panels in figure 9) and precipitation rate (GPCP; lower panel in figure 9). Though zonal wind anomalies are similar in the residuals A, B, C and D at 850 mb (fig 9 a3-d3), the precipitation rate anomalies are positive only in C and D (fig 9 c4-d4) over southeastern coast of

India, northern Sri Lanka, the southwestern part of the BOB, and over the Indian Ocean. However, negative anomalies of precipitation rate persist in the residuals A and B (fig 9 a4-b4) over the same regions. This kind of dissimilarity in precipitation rate even in the presence of similar kind of anomalous wind fields is questionable. To get contrasts among the composites A, B, C, and D it is important to have an appropriate understanding of the each residual. As mentioned earlier, the A residual is a difference between EC and NC waves. The presence of anomalous easterlies at 850 mb in (fig 9 a3) exhibits the dominating nature of EC wave over the NC wave. As a result, dryness due to less precipitation is witnessed over the Indian Ocean and southeastern India (fig 9 a4). A similar situation persists in the residual B, which is a difference between EC and MC wave, where a leftover wave of El Nino dominates. As a result, southwestern peninsular India, and northern Sri Lanka show significant positive anomalies of rainfall (fig 9 b4). Likewise, easterlies at 850 mb are stronger in B (fig 9 b3) residual than in A, which conveys the importance of leftover El Nino wave and its domination over the MC wave. The C residual is the remnant of blended wave EMC with Normal wave, and, D residual is the balance of EMC wave with MC wave. In C residual, EMC wave dominates in the foreground, whereas, in D residual El Nino wave controls the foreground. In both of these residuals, strong easterlies dominate at 850 mb over the Indian Ocean (fig 9 c3 and fig 9 d3), which might cause wetness over the southeastern coast of India, southwestern BOB, and the Indian Ocean regions (fig 9 c4 and fig 9 d4).

In addition to easterlies at lower tropospheric levels in residuals A, B, C and D, the upper tropospheric wind fields like subtropical westerlies (STW) at 200 mb (fig 9 a1-d1) and 500 mb levels (fig 9 a2-d2) could have moderately influenced the weather of southern India. These residuals showed very clear cyclonic circulations in STW. Due to relatively strong nature of

435 STW's, its influence extended equatorward up to South India. This deepening of trough related
436 to STW triggered the transport of moisture from the south BOB to northwards, which might be
437 another reason for positive precipitation anomalies over South India in C and D residuals. These
438 striking aspects of STW are in agreement with the results obtained by Li C et al. (2015).
439 Moreover, the strength of STW is more in D composite (fig 9d1) than in any other composites,
440 which clearly implies the remnant El Nino wave is relatively strong in D residual than in any
441 other residuals.

442 An interesting situation attains with residual F, in which the remnant of EMC blended
443 wave and EC wave is MJO wave. The remnant MJO wave is appreciably seen over the equator
444 around 80^{o}E as strong westerly anomalies at 850 mb (fig 9 f3) and strong easterlies at 200 mb
445 (fig 9 f1). In the F residual, whole central India is quietly dry, whereas, southeastern India (Tamil
446 Nadu coast, and Andhra Pradesh coast) and North Sri Lanka shows a significant positive
447 anomaly of precipitation rate of the order 1-2 mm/day (fig 9 f4). The extraordinary amount of
448 precipitation over the coast of southeastern India can be essentially attributed to the residual
449 wave F, which propagates over the background El Nino low-frequency wave, and MC wave.
450 Also, over the Indian Ocean, significant positive anomalous precipitation is observed in F
451 residual. It implies that the blended EMC wave interacts with the background EC wave to cause
452 anomalous precipitation over the regions mentioned above. Consequently, this kind of the
453 distinctive features of EMC blended wave and EC wave interactions was noticed during the
454 extreme events of 2015 OND season, which caused extreme precipitation over the southeastern
455 India. The residual E also shows a pattern which is similar to that of F residual, but westerly
456 wind strength at 850 mb and 500 mb is too weak (fig 9 e3 & 9 e2). The strength of upper
457 tropospheric easterlies at 200 mb (fig 9 e1) is feeble, and southern India appears to be dry due to

lack of precipitation (fig 9 e4). Nevertheless, a significant amount of precipitation is observed over the Indian Ocean in E residual. Moreover, the upper tropospheric strong easterlies weaken the subtropical westerlies (STW) in both E and F residuals (fig 9 e1 & 9 f1). The weakening of STW in these residuals is attributed to the anticyclonic circulations, which could be another reason for dryness over northern and central India in the residuals E and F. Thus; these residuals are necessary in the case of blended EMC waves over a region.

3.7 The vertical cross-section of zonal and meridional circulations in the residuals.

The vertical cross-section of the longitudinal variations of relative humidity and omega (weighted by zonal winds) from 20^{o}E to 280^{o}E averaged over latitude 5^{o}S to 5^{o}N are illustrated for A, B, C, D, E, and F residuals in figure 10, which depicts the different branches of the Walker circulation. These various branches of Walker circulation over the equator is demonstrated by Bjerknes (1969) and Walker et al. (1932). The subsidence of dry and stable air over the central Pacific Ocean is observed in residuals E (fig 10e) and F (fig 10f), whereas rising limb of moist air is witnessed over the same region in the residuals A, B, C and D (figure 10a to 10d respectively). The above-mentioned zonal circulation in residual E is associated with the normal Walker Circulation with rising branch over maritime continent and descending branch over central and the eastern Pacific Ocean, but the same circulation in residuals A, B, C, and D are affected by atmospheric variability mainly El Nino. Due to the effect of El Nino, the rising branches of moist air in residuals A, B, C, and D over the Indian Ocean are weakened except over the East African coast, which is the case of Walker Circulation variability due to El Nino as explained by Philander (1990). Furthermore, subsidence of dry air over the maritime continent and ascending moist air over the Indian Ocean is perceived in the residuals E and F. However, in the residuals A, B, C, and D rising limb of moist air exists over the western Indian Ocean and

481 subsidence of dry wind over the maritime continent and the eastern Indian Ocean. Besides, the
482 ascending moist wind is recognized over the Indian Ocean in residuals E and F. Exceptionally in
483 residual F; the rising branch is healthy around 80^{o}E. Consequently, the ascending limb at 80^{o}E in
484 residual F well matches with the ascending limb over the Indian Ocean during November 8 to
485 17, 2015 as shown in figure 5c. Hence, anomalous Walker circulation branch could account the
486 significant positive rainfall anomalies over southern India, which is in agreement with the studies
487 of Allan et al. (1986).

488 Similarly, a latitudinal variation of relative humidity and Omega from 30^{o}S to 30^{o}N
489 averaged over 75^{o}E to 85^{o}E is shown in figure 11. It displays the meridional overturning Hadley
490 circulation (HC; Held et al., 1980) variations among the residuals. The residuals of E (fig 11e)
491 and F (fig 11f) shows the standard Hadley circulation with rising branch over the equator and
492 subsidence over the subtropics around 30^{o}S & 30^{o}N. However, the residuals of A, B, C, and D
493 (fig 11a to 11d) shows ascending moist air over the equator with less meridional extent, and a
494 strong rising of moist air is noticed around 30^{o}S & 30^{o}N. The sturdy ascent over subtropics is
495 associated with the impact of El Nino, which strengthened the STW as explained before; these
496 observations over subtropics are in agreement with the studies of Seager et al. (2003).
497 Interestingly, in the residuals of E and F, rising moist air is identified over the tropics around
498 10^{o}N to 15^{o}N and is much stronger in F residual. Therefore, a healthy ascent of moist air in
499 residual F matches with the ascent over the Indian Ocean during November 8 to 17 in 2015.
500 Strikingly, these results elicit the large-scale variability of the atmosphere in both meridional and
501 zonal circulations, which appreciably affected the local weather of southern India with the
502 transport of moist air.

503 **3.8 The response of precipitation to residual waves.**

The current section focuses on the response of precipitation over southeastern India to the zonal winds in the residual waves. Figure 12 summarizes the precipitation rate (averaged over 8^oN-16^oN & 75^oE-85^oE) responds to the zonal wind anomalies (averaged over the regions 0^o-6^oN & 70^oE-80^oE for MJO wave and 2^oS-4^oN & 90^oE-98^oE for El Nino wave) of composites NC, MC, EC, and EMC. The motive behind in selecting different regions for MJO and El Nino is to showcase the domination of westerly wind anomalies in residuals E and F for MJO region, and easterly wind anomalies in A, B, C, and D residuals for El Nino region. A linear relationship was constructed between zonal wind anomalies and precipitation rate of each composite. In the case of NC composite, the response of precipitation to the change in zonal wind anomalies is steady, which is apparent from the noticeable correlation coefficient of 0.086. Whereas, MC composite precipitation response to the zonal wind anomalies seems to fluctuate with a reasonable standard deviation of 3.32 and a moderate correlation of 0.26. Notably, on some occasions, strong westerlies over the region for MJO showed high precipitation response over southeastern India, but when individual events are examined, the response of precipitation over the same region is weak, which makes MC composite quite trivial. Interestingly, in EC composite, the zonal wind anomalies and precipitation rate is considerably positively correlated with a correlation of 0.97 and sensible standard deviation of 1.26, with dominated easterlies. As a result, precipitation responds appreciably positive to the strength of easterlies, which markedly causes more wetness over the southeastern India. However, there are some events of easterlies, with weak precipitation response and sometimes dryness over the southeastern India.

In the blended EMC wave, the response of precipitation rate anomalies to the zonal wind anomalies exhibited dual nature with a correlation coefficient of 0.05. In the dual nature of EMC wave, the precipitation response of dominated EC wave is high as compared to the dominated

MC wave. In the past, very few such EMC wave cases are noticed during OND season. An interesting situation was achieved, wherein, residuals C, D, and F showed the strong response of precipitation to the easterly wind anomalies in C, D, and westerly wind anomalies in F. As a result, F residual significantly suppresses the easterlies of EC wave, and gives rise to the MC wave from EMC blended wave to dominate in the foreground. Consequently, precipitation responds substantially to the westerly zonal wind anomalies, which causes rain over the southeastern India. The other residuals do not respond like F residual, but they too are necessary for additional interactions among composite waves, and their corresponding precipitation response. Remarkably, residual D with prevailing easterlies responds with high rainfall over the southeastern India like in F, but in the case of remaining residuals precipitation decreases over the same region. With the background of composite wave and residual wave interactions, their precipitation responses, leads to a hypothesis. The hypothesis states that 'beforehand, if there is a prevailing moderate to very strong El Nino in the background as a low-frequency wave (EC), and, if another high-frequency wave like MJO propagates over the background (MC) in the equatorial Indian Ocean during October – December season, then the blended wave EMC interacts with prevalent EC wave. This interaction creates a remnant wave MJO, which dominates in the foreground of EC wave. This remnant MJO wave considerably suppresses the effect of background EC wave by weakening easterlies at 850 mb and replacing it with very strong westerlies around 80^{o} E near to equator like in F residual. Eventually, remnant MJO wave, in turn, affects the weather of southeastern India with the development of mesoscale convective systems, which contributes extreme precipitation as a positive response over the same region and neighboring regions'. Such a unique behavior and make-up of F residual are not accompanied with any other residuals. As a result, the residual F is unique in nature, and such cases are

infrequent in the past. Similar analysis is performed quantitatively by stretching the analysis period to 1981-2014 (here, NCEP precipitation rate is used instead of GPCP because GPCP data set is available only until 1997) so that another strong El Nino case is included in the study and the number of samples of data would be more. This quantitative analysis also accomplishes similar results as seen in the previous qualitative study with GPCP observations. Therefore, these two types of analysis demonstrate the robustness of the hypothesis. It clearly indicates the domination of blended wave EMC over background state El Nino wave. Therefore, blended El Nino & MJO wave has shown two different kinds of convolutions. Firstly, mixed wave dominates the foreground MJO wave in residual E, and secondly, mixed wave dominates background El Nino wave in F residual. As a result, the domination of mixed wave over El Nino and MJO states requires special attention.

4. Summary

In this work, extreme precipitation events during the northeast monsoon season of 2015 were analyzed. Extreme rainfall associated with case-1 is connected to the deep tropical depression formed over the northern Indian Ocean. The case -2 event is related to the LPA, and case-3 rain event is due to the UAC over southern India. This analysis also ignited an outlook that tropical variability could influence the wind fields, which can alter the carrier of moisture in OND season from northeasterly winds to southerly winds.

The power spectrum analysis of meteorological variables during winter monsoon of 2015 over NEM region revealed the significant dominant periodicities of 30-40 days in some of the variables like mid-tropospheric humidity, zonal wind at 200 mb and soil moisture. Likewise, another important periodicity of 2-17 days was seen with most of the variables. Subsequently, these dominant periodicities are filtered for MJO (30-90 days), Kelvin and equatorial Rossby waves in the anomalies in the zonal wind at 850 mb and 200 mb, precipitation rate, sea level pressure and velocity potential. These filtered atmospheric variables illuminated the dominant mode of tropical variability as MJO and associated CCEWs, which influenced the weather over southern India by enhanced convection. Though MJO appeared weak during the extreme events, its remnants interacted with the background atmosphere. One of the important observations is, though El Nino is very strong propagating in the background atmosphere in 2015 during OND season, its influence is suppressed over the Indian Ocean by remnants of MJO & associated CCEWs with very vigorous westerly winds. This kind of interaction is uncommon in the past episodes of El Nino; as a result, the interaction of El Nino and remnants of MJO & associated CCEWs during winter monsoon of 2015 engraved its identity in the literature.

Further, a composite analysis of past extreme precipitation events of moderate to strong El Nino events, active MJO events, and Normal events from 1997-2014 in OND season is exploited to study the interactions of El Nino wave with El Nino & MJO blended wave (F residual). This kind of interaction resulted in a hypothesis that, if El Nino prevailing as background low-frequency wave, superimposed with high-frequency MJO over the Indian Ocean during OND season, then blended El Nino & MJO wave could suppress the easterlies of El Nino wave by replacing with westerlies, which are remnants of MJO, in turn causes extreme precipitation over the southern India. The influence of residuals on vertical cross-sections of relative humidity and Omega revealed an anomalous branch of the Walker circulation over the Indian Ocean in F residual of El Nino & MJO and El Nino composite wave, which nourished the moisture to the mesoscale convective systems formed over southern India. Similarly, latitudinal variations showed an anomalous meridional circulation over the southern India around 10^{o} N to 15^{o} N, which also fed moisture to the mesoscale convective systems over the region mentioned above. Also, the meridional flow of humidity to the western edge of subtropical anticyclones, transport moisture from the equatorial Indian Ocean to subtropics, which is revealed from the analysis of F residual (obtained from historical extreme events analysis) and also found in case-1, case-2, and case-3 events. This transport of moisture could feed the mesoscale convective systems over southern India. As a result, current investigation very clearly depicts the importance of the residual F during mesoscale convective systems over the southeastern Indian region in intra-seasonal scale. Fruitfully, it explains the kind of tropical variability, occasional interactions between El Nino & MJO, and large-scale phenomenon behind the extreme events over southern India. The co-existence of MJO and El Nino is a general phenomenon seen over tropical regions, but the interactions in which MJO masks out the effects of El Nino is crucial.

The evidence related to such suppression of El Nino by MJO is very slim in literature. Sensitivity studies could be helpful in the supplementary understanding of the interaction between El Nino & MJO. Such studies will be essential in the prediction of extreme events associated with those different interactions of El Nino and MJO. A systematic, detailed study of interactions of El Nino and other CCEW like Kelvin wave and equatorial Rossby wave, during winter monsoon, would be investigated in future, which will fill gaps in the tropical variability study of NEM over the Southern Indian region. Lastly, this year's unique interaction between a well-developed, strong El Nino and MJO wave is a textbook example of the scientific society, and it began in the Indian Ocean and caused extreme precipitation events over southeastern India.

634 **Acknowledgements**

635 This work is a part of the INCOMPASS project 2015-2018 supported by Ministry of
636 Earth Sciences (MoES). Both of the authors are obliged to the Director CSRI National
637 Aerospace Laboratories (CSIR-NAL) and Head Centre for Electromagnetics Department (CEM)
638 Bangalore India, for providing facilities and support. The lead author Mr. Rakesh Teja Konduru
639 is grateful to MoES for providing research fellowship in the INCOMPASS project. The authors
640 also thankful to co-researcher for their help in preparing research draft.

641

642

643

644

645

646

647

648

649

650

651

652

References

Bjerknes, J., 1969. Atmospheric teleconnections from the equatorial Pacific. Mon. Weather Rev. *V*ol 97, 3,163-172.

Dhar, O. N., Rakhecha P. R., 1983. Forecasting northeast monsoon rainfall over Tamil Nadu, India. Mon. Weather Rev. 111, 109-112.

Dunkerton, T. J., Crum, F. X., 1995. Eastward propagating 2-15 day equatorial convection and its relation to the tropical intraseasonal oscillations. J. Geophys. Res. 100, 25781-25790.

Entin, J. K., Robock, A., Vinnikov, K. Y., Hollinger, S. E., Liu, S., Namkhai, A., 2000. Temporal and spatial scales of observed soil moisture variations in extratropics. J. Geophys. Res. 105, 11865-11877.

Gottschalck, J., Wheeler, M., Weickmann, K., Vitart, F., Savage, N., Lin, H., Hendon, H., Waliser, D., Sperber, K., Nakagawa, M., Prestrelo, C., Flatau, M., Higgins, W., 2010. A Framework for Assessing Operational Madden-Julian oscillation forecasts: A CLIVAR MJO working group project. Bull. Amer. Meteor. Soc. 91,9, 1247-1258.

Guhathakurta, P., Sreejith, O. P., Menon, P. A., 2011. Impact of climate change on extreme rainfall events and flood risk in India. J. Earth Sys. Sci. 120(3), 359-73.

Guo, Y., Jiang, X., Waliser, D. E., 2014. A Systematic Relationship between the Representations of Convectively Coupled Equatorial Wave Activity and the Madden-Julian Oscillation in the Climate Model Simulations. *J. Clim.* 28, 1881-1904.

Held, I. M., Hou, A. Y., 1980. Nonlinear axially symmetric circulations in a nearly inviscid atmosphere. J. Atmos. Res. 37, 515-533.

674 Hendon, H. H., Wheeler M. C., Zhang C., 2007. Seasonal dependence of the MJO-ENSO
675 relationship. *J. Clim.* 20, 531-543.
676 Hou, A. Y., Kakkar, R. K., Neeck, S., Azarbarzin, A. A., Kumerrow, C. D., Kojima, M., Oki,
677 R., Nakamura, K., Iguchi, T., 2014. The global precipitation measurement mission. Bull.
678 Am. Meteor. Soc. 95, 701-22.
679 Huffman, Adler G. J. R. F., Morrissey, M. M., Curtis, S., Joyce, R., McGavock, B., Susskind, J.,
680 2001. Global precipitation at one-degree daily resolution from multi-satellite
681 observations. J. Hydrometeorology, 2, 36-50.
682 Jia, X., Chen, L. J., Ren, F. M., Li, C. Y., 2011. Impacts of the MJO on winter rainfall and
683 circulation in China. Adv. Atmos. Sci. 28(3), 521-533, doi:10.1007/s00376-010-9118-z.
684 Kalnay, E., Kanamitsu, M., Kistler, R., Collins, W., Deaven, D., Gandin, L., Iredell, M., Saha,
685 S., White, G., Woollen, J., Zhu, Y., Leetmaa, A., Reynolds, R., Chelliah, M., Ebisuzaki,
686 W., Higgins, W., Janowiak, J., Mo, K. C., Ropelewski, C., Wang, J., Roy Jenne, Dennis
687 Joseph, 1996. The NCEP/NCAR 40-year reanalysis project. Bull. Amer. Meteor. Soc. 77,
688 437-470.
689 Kiladis, G. N., Wheeler, M., 1995. Horizontal and vertical structure of observed tropospheric
690 equatorial Rossby waves. J. Geophys. Res. 100(D11), 22981-22997.
691 Kiladis, G. N., Wheeler, M. C., Haertel, P. T., Straub, K. H., Roundy, P. E., 2009. Convectively
692 coupled equatorial waves. Rev. Geophys. 47.
693 LI , C., Sun, J. L., 2015. Role of the subtropical westerly jet waveguide in a southern China
694 heavy precipitation in December 2013. Adv. Atmos. Sci. 32(5), 601-612.

695 Liebmann, B., Hendon, H. H., Glick, J. D., 1994. The relationship between the tropical cyclones
696 of western Pacific and the Indian Ocean and Madden-Julian Oscillation. J. Meteor.Soc.
697 Japan, 72 401-412.
698 Madden, R. A., Julian, P. R., 1971. Detection of a 40-50 day Oscillation in the Zonal Wind in the
699 Tropical Pacific. J. Atmos. Sci. 28, 702-708.
700 Majda, A. J., Khouider, B., Kiladis, G. N., Straub, K. H., Shefter, M. G., 2004. A model for
701 convectively coupled tropical waves: Nonlinearity, rotations and comparison with
702 observations. J. Atmos. Sci. 61, 2188-2205.
703 Mapes, B., Tulich, S., Lin, J., Zuidema, P., 2006. The mesoscale convective life cycle: building
704 block or prototype for large-scale tropical waves? Dyn. Atmos. Oceans, 42, 3-29.
705 Mitra, A. K., Dasgupta, M., Singh, S. V., Krishnamurti, T. N., 2003. Daily rainfall for Indian
706 monsoon region from merged satellite and rain gauge values. J. Hydrometeorology, *4(5)*,
707 769-781.
708 Mitra, A. K., Bohra A. K., Rajeevan M. N., and Krishnamurti T. N., 2009: Daily Indian
709 precipitation analysis from a merge of rain-gauge data with the TRMM/TMPA satellite-
710 derived rainfall estimates. *J. Meteorol. Soc. Jap.,* Vol. 87A, 265-279.
711 Mitra, A. K., Mornin, I. M., Rajagopal, E. N., Basu, S., Rajeevan, M. N., Krishnamurti, T. N.,
712 2013b. Gridded daily Indian monsoon rainfall for 14 seasons: Merged TRMM and IMD
713 gauge analyzed values. J. Earth Sys. Sci. 122(5), 1173-1182.
714 Nageswara Rao, G. 1999. Variations of the SO Relationship with Summer and Winter Monsoon
715 Rainfall over India: 1872-1993. J. Clim. 12, 3486-3495.

716 Nakawaza, T., 1988. Tropical superclusters within intraseasonal variations over the western
717 pacific. J. Meteor. Soc. Japan, 66, 823-839.
718 Pankaj, Kumar, Rupa Kumar, K., Rajeevan, M., Sahai, A. K., 2007. On the recent strengthening
719 of the relationship between ENSO and northeast monsoon rainfall over South Asia. Clim.
720 Dyn. 8, 649-660.
721 Pattanaik, D. R., Rajeevan, M., 2010. Variability of extreme rainfall events over India during
722 southwest monsoon season. Meteorol. Appl. 17, 88-104.
723 Philander, S. G., 1990. El Nino, La Nina, and the Southern Oscillation. 293 pp, Academic, New
724 York.
725 Rajeevan, M., Unnikrishnan, C. K., Jyoti Bhate, Niranjan Kumar, K., Sreekala, P. P., 2012.
726 Northeast monsoon over India: variability and prediction. Meteorol. Appl. 19, 226-236.
727 Ropelewski, C. F, Halpert, M. S., 1989. Precipitation pattern associated with the high index
728 phase of the Southern Oscillation. J. Clim. 2, 268-284.
729 Ropelewski, C. F., Halpert, M. S., 1987. Global and regional scale precipitation patterns
730 associated with the El Nino/Southern Oscillation. Mon. Wea. Rev. 115, 1606-1626.
731 Roundy, P. E., William Frank, M., 2004a. A climatology of waves in the Equatorial region. J.
732 Atmos. Sci. 61, 2105-2132
733 Roundy, P. E., William Frank, M. 2004b. Effects of low-frequency wave interactions on
734 intraseasonal oscillations. J. Atmos. Sci. 61: 3025-3040
735 Roundy, P. E., Kiladis, G. N., 2006. Observed relationship between oceanic Kelvin waves and
736 atmospheric forcing. J. Clim. 19, 5253-5272.

737 Roundy, P. E., 2008. Analysis of convectively coupled Kelvin waves in the Indian Ocean MJO.
738 J. Atmos. Sci. 65,4, 1342-1359
739 Satya Prakash, Mitra, A. K., Pai, D. S., Amir Agha Kouchak, 2015. From TRMM to GPM: How
740 well can heavy rainfall be detected from space? Adva. Water Res. 88, 1-7.
741 Seager, R., Harnik, N., Kushnir, Y., Robinson, W., Miller, J., 2003. Mechanisms of
742 hemispherically symmetric climate variability. J. Clim. 16, 2960-2978.
743 Straub, K. H., Kiladis, G. N., 2002. Observations of convectively coupled Kelvin wave in the
744 eastern Pacific ITCZ. J. Atmos. Sci. 59, 30-53.
745 Straub, K. H., George Kiladis, N. 2010. Observations of a Convectively Coupled Kelvin Wave in
746 the Eastern Pacific ITCZ. J. Atmos. Sci. 59, 30-53.
747 Suppiah, R., 1997. Extremes of Southern Oscillation phenomenon and the rainfall of Sri Lanka.
748 Int. J. Climatol. 17, 87-101.
749 Takayabu, Y. N., Murakami, M., 1991. The structure of super cloud clusters observed in 1-20
750 June 1986 and their relationship to easterly waves. J. Meteor Soc. Japan, 69, 105-125.
751 Vinnikov, K. Y., Yeserkepova, I. B., 1991. Soil moisture, empirical data and model results. J.
752 Clim. 4, 66-79.
753 Vinnikov, K. Y., Robock, A., Speranskaya, N. A., Schlosser, A., 1996. Scales of temporal and
754 spatial variability of midlatitude soil moisture. J. Geophys. Res. 101, 7163-7174.
755 Walker, G. T., Bliss, E., 1932. World Weather. V. Mem. Roy. Met. Soc. *4, 53-84.*
756 Wang, B., 2002. Kelvin Waves., doi:10.1006/rwas.2002.0191.
757 Wheeler, M., Kiladis, G. N., 1999. Convectively coupled equatorial waves: Analysis of clouds

758 and temperature in the wavenumber-frequency domain. J. Atmos. Sci., 56, 374-399.
759 Wheeler, M., Kiladis, G. N., Webster, P. J., 2000. Large-scale dynamical field associated with
760 the convectively coupled equatorial waves. J. Atmos. Sci. 57, 613-640
761 Wheeler, M. C., Hendon, H. H., 2004. An all-season real-time multivariate MJO index:
762 development of an Index for monitoring and prediction. Mon. Wea. Rev. 132, 1917-1932.
763 Zhang, C., 2005. Madden-Julian oscillation. Rev. Geophys. 43.
764 Zubair, L., Ropeleswski, C. F., 2006. The strengthening relationship between ENSO and
765 northeast monsoon rainfall over Sri Lanka and southern India. J. Clim. 19, 1567-1575.
766 Allan, R. J., Lindesay, J., Parker, D., 1996. El Nino Southern Oscillation and Climatic
767 Variability., 402 pp., CSIRO, Collingwood, Victoria, Australia.
768 Climate Prediction Center (CPC) Oceanic Nino Index. 2006., Climate Prediction Center,
769 National Centers for Environmental Prediction, national Weather Service, U.S.
770 Department of Commerce, Maryland.
771 Consensus statement on the Forecast for the 2015 Northeast Monsoon Season (October –
772 December) Rainfall and Temperature over South Asia. First Session of Winter South
773 Asian Climate Outlook Forum (WinSASCOF-1). Chennai, India. October 15-17 2015.
774 The NCAR Command Language (Version 6.3.0) [Software]. 2016, Boulder, Colorado:
775 UCAR/NCAR/CISL/TDD. http://dx.doi.org/10.5065/D6WD3XH5.
776 Tropical Rainfall Measurement Mission Project (TRMM). 2011, TRMM/TMPA 3B42RT 3
777 Daily TRMM and Others Daily Rainfall Estimate V7. Goddard Space Flight Center
778 Distributed Active Archive Center (GSFC DAAC), Greenbelt, MD.

779 Table 1: Extreme rainfall events from 1981-2014 in OND were selected based on criteria if daily rainfall
780 is more than 64.5 mm. The events from 2000-2014 are confirmed based on the India Meteorological
781 Department weather reports. Here, yellow color represents extreme rain events related to El Nino & MJO.

S.No.	Years	Heavy rainfall events
1	1981	**Oct 26-29**
2	1982	**Oct 17-21, Nov 2-6**
3	1985	Nov 19-24, Dec 13-15
4	1986	**Oct 3-6,Oct 29-Nov 3**, Oct 5-7
5	1987	Oct 16-17, **Nov 3-5,** Nov 13-14, **Dec 5-7**
6	1989	Dec 2-4, Nov 11-14, Oct 7-9
7	1990	Oct 1-3, **Oct 23-25**, **Oct 29-Nov 4**, Nov 26-27
8	1991	Oct 28-Nov 1, Nov 13-18
9	1992	**Oct 4-5**, Oct 9-11, Nov 14-19
10	1993	Oct 8-12, Oct 31-Nov 1, **Nov 6-12**, **Nov 24-25**, Dec 24-26
11	1996	Oct 1-5, Oct 9-15, **Oct 17-21**, Nov 8-9, **Nov 21-26**, **Dec 7-16**
12	1997	Oct 12-16, Oct 21-25, Oct 28-29, Nov2-8, **Nov 14-18**, Nov 26-27, **Dec 3-8**
13	1999	**Oct 1-6**, **Oct 14-15**, Nov 18-21, **Nov 27-29**, Dec 21-22
14	2001	Oct 5-6, Oct 15-16, **Nov 5-7**, Dec 21-22
15	2002	Oct 7-15, **Oct 25-30**, **Nov 5-10**, Dec 6

16	2003	Oct 19-21, Dec 15, Dec 24
17	2005	**Oct 8-9**, **Oct 10-15**, Oct 18-19, Oct 21-24, Nov 4-8, Nov 20-24, Dec 2-3, **Dec 9-10**
18	2008	**Oct 13-16**, Oct 20-26, Nov 16-17, Nov 23-30, Dec 9-11
19	2009	Oct 1-4, Oct 29-30, **Nov 3-9**, Nov 15-16, Dec 2-4, Dec 14-16
20	2012	Oct 1-3, Oct 6-7, Oct 13-15, Oct 19-22, **Oct 31-Nov 4**, **Dec 3-5**
21	2013	Oct 20-26, Nov 2-4, **Nov 16-18**, Nov 24-28, Dec 12-13
22	2014	Oct 9-13, Oct 17-19, **Oct 26-27**, Nov 13-15, **Nov 21-22**, Dec 29-30

792

793 Table 2: The composites of Normal, El Nino, MJO events and their combinations.

S.NO.	Composites	No. of Events
1	Normal	47
2	Normal & MJO	21
3	El Nino	17
4	El Nino & MJO	11
	Total	96

794

795

796

797

798

799

800

801

802

803

List of Figures

Figure 1: Top row in the panel is composite of GPM precipitation rate (mm/day) and below row in the panel is TRMM 3B42RT precipitation rate during the three cases, i.e., case-1 (left-most column), case-2 (middle column), and case-3 (right most column). The dashed contour are NCEP sea level pressure negative anomalies and solid contour are NCEP sea level pressure positive anomalies. Those Vectors represent NCEP wind field anomalies.

Figure 2: These plots are drawn over latitude 12^{o}N-13^{o}N and longitude 80^{o}E which covers Chennai region of India from October 1 to December 31 of 2015. a) NCEP precipitation rate (mm/day) averaged over the mentioned region. b) The red color solid line is NCEP lifted index and green color solid line are NCEP sea level pressure, c) NCEP omega anomalies are, d) NCEP zonal wind anomalies, and e) NCEP relative humidity anomalies. Note NCEP relative humidity is available up to 300 mb. All of these variables were composited for case-1 (Nov 9-Nov 10), case-2 (Nov 15-Nov 16), and case-3 (Nov 30-Dec 2), which are mentioned as black color dashed vertical lines.

Figure 3: NCEP zonal wind anomalies composite is created for three cases i.e. (a-d-g) case-1 (Nov 9 to 10), b-e-h) case-2 (Nov 15 to 16), and c-f-i) case-3 (Nov 30-Dec 2). Each row of the panel represents a pressure level, which is shown to the right of the last column of the panel. A lowermost row of the panel corresponds to the zonal wind anomalies at 850 mb, and a topmost row of the panel represents 200 mb zonal wind anomalies. Shaded portion is zonal wind anomalies and vectors are anomalous wind. The solid contours are positive velocity potential anomalies, and dashed lines are negative velocity potential anomalies contoured from - 6 to 6 with an interval of three.

Figure 4: The NCEP meridional wind (m/s) anomalies composite is created for three cases i.e. (a-d-g) case-1 (Nov 9 to 10), b-e-h) case-2 (Nov 15 to 16), and c-f-i) case-3 (Nov 30-Dec 2). Each row of the panel represents a pressure level, which is shown to the right of the last column of the panel. A lowermost row of the panel corresponds to the meridional wind anomalies at 850 mb, and a topmost row of the panel

represents 200 mb meridional wind anomalies. Shaded portion is meridional wind anomalies and vectors are anomalous wind. The solid contours are positive relative humidity (%) anomalies contoured from -50 to 50 with an interval of 15. Note NCEP Relative Humidity data is available only up to 300 mb pressure levels.

Figure 5: It demonstrates vertical cross-sections of omega, and relative humidity. Left column shows longitudinal cross-section (a, c) and right column (b, d) represents latitudinal cross-sections. Longitudinal cross-sections are averaged over 5^{o}S-5^{o}N, and latitudinal cross-sections are averaged over 75^{o}E-85^{o}E. Top row (a, b) represents OND anomalies, and bottom row shows (c, d) mean of the composite from November 8 to 17, 2015. Here vectors are omega values scaled w.r.t to zonal wind for longitudinal section and meridional for latitudinal section

Figure 6: Power spectrum is shown for a) TRMM 3B42 precipitation rate, b) NCEP precipitation rate, c) air temperature, d) zonal wind at 850 mb, e) soil moisture at 0-10 cm, and f) Omega at 850 mb, during October-December of 2015 over southern Indian region (8^{o}N-20^{o} N & 70^{o}E-85^{o}E) is calculated. Green Line shows Markov Red Noise spectrum; red line show upper 95% confidence bounds; and the blue line shows lower 5% bounds. The x-axis represents periodicity and y-axis represents variance.

Figure 7: It displays MJO band pass filtered NCEP zonal wind (m/s) anomalies composite is created for three cases i.e. (a-d-g) case-1 (Nov 9 to 10), b-e-h) case-2 (Nov 15 to 16), and c-f-i) case-3 (Nov 30-Dec 2). Each row of the panel represents a pressure level, which is shown to the right of the last column of the panel. A lowermost row of the panel corresponds to the meridional wind anomalies at 850 mb, and a topmost row of the panel represents 200 mb meridional wind anomalies. Shaded portion and vectors are band-pass filtered (30-90 days) zonal wind anomalies. In the bottom panel, the dashed contours are negative sea level pressure (mb) anomalies and solid contours are positive sea level pressure anomalies contoured for -0.3, -0.1, and 0.3. In the first panel, the dashed contour is a negative velocity potential anomaly, and the solid line is positive velocity potential anomaly contoured for -4.0, -0.5, 0.5, and 4.0.

852 **Figure 8:** It display Hovmueller plots of band-pass filtered (30-90 days for MJO, 9-72 days for equatorial
853 Rossby waves, and 2.5-17 days for Kelvin waves) a) zonal wind anomalies at 850 mb (m/s), b) zonal
854 wind anomalies at 200 mb (m/s) and c) NCEP precipitation rate (mm/day), they are averaged over 10^{o}S-
855 10^{o}N. Shaded portion represents MJO filtered waves. Whereas, blue color solid line and red color solid
856 line represent Kelvin waves and equatorial Rossby waves respectively. Dotted black line points the dates
857 during which case-1, case-2, and case-3 happened.

858 **Figure 9:** It summarizes the residuals, which are difference between (A) E and N composite (left
859 column), (B) E and M composite, (C) EM blended and N composite, (D) EM blended and M composite,
860 (E) M and N composite, and (F) EM blended and E composite; for NCEP zonal wind anomalies (m/s) and
861 GPCP precipitation rate (mm/day) anomalies. Each row of the panel represents a pressure level, which is
862 shown to the right of the last column of the panel. A lowermost row of the panel corresponds to the wind
863 anomalies at 1000 mb, and precipitation rate anomalies and a topmost row of the panel represents 200 mb
864 zonal wind anomalies. The shaded portions of a second bottom row of the panel to top most rows are
865 zonal wind anomalies. In all of the plots only, more than 95 % significant values are shown (Student's t-
866 test is performed at critical value 0.05).

867 **Figure 10**: It summarizes the zonal vertical cross-sections of omega, and relative humidity anomalies of
868 A, B, C, D, E, and F residuals, which are differences of E & N, E & M, EM & N, EM & M, M & N and
869 EM & E composites, and these composites are explicitly discussed in section 3.6. These longitudinal
870 cross-sections were averaged over 5^{o}S-5^{o}N. Here vectors are omega values scaled w.r.t to the zonal wind,
871 and colored region shows relative humidity anomalies.

872 **Figure 11**: It describes the meridional vertical cross-sections of omega, and relative humidity anomalies
873 of A, B, C, D, E, and F residuals, which are differences of E & N, E & M, EM & N, EM & M, M & N,
874 and EM & E composites, and these composites are explicitly discussed in section 3.6. These latitudinal

875 cross-sections are averaged over 75°E-85°E. Here vectors are omega values scaled w.r.t to the meridional
876 wind, and colored area shows relative humidity anomalies.

877 **Figure 12**: It demonstrates the response of GPCP precipitation anomalies to NCEP zonal wind anomalies
878 in MJO (red; M), Normal (green; N), El Nino (blue; E) and El Nino & MJO mixed wave (magenta; EM)
879 composites. Here composites are created for a period 1997-2014 in OND season. The black color markers
880 represent the residuals A, B, C, D, E, and F; these residuals are interactions of M & N, E & N, E & M,
881 EM & N, EM & M and EM & E composites respectively. The precipitation anomalies shown above are
882 area averaged over 8°N-16°N & 75°E-84°E, and zonal wind anomalies are area averaged over 0°-6°N &
883 70°E-80°E for MJO and 2°S-4°N & 90°E- 98°E for El Nino composites. The statistical characteristics like
884 p-value (p), correlation coefficient (r), and standard deviations (std) of each composite are also shown in
885 the figure.

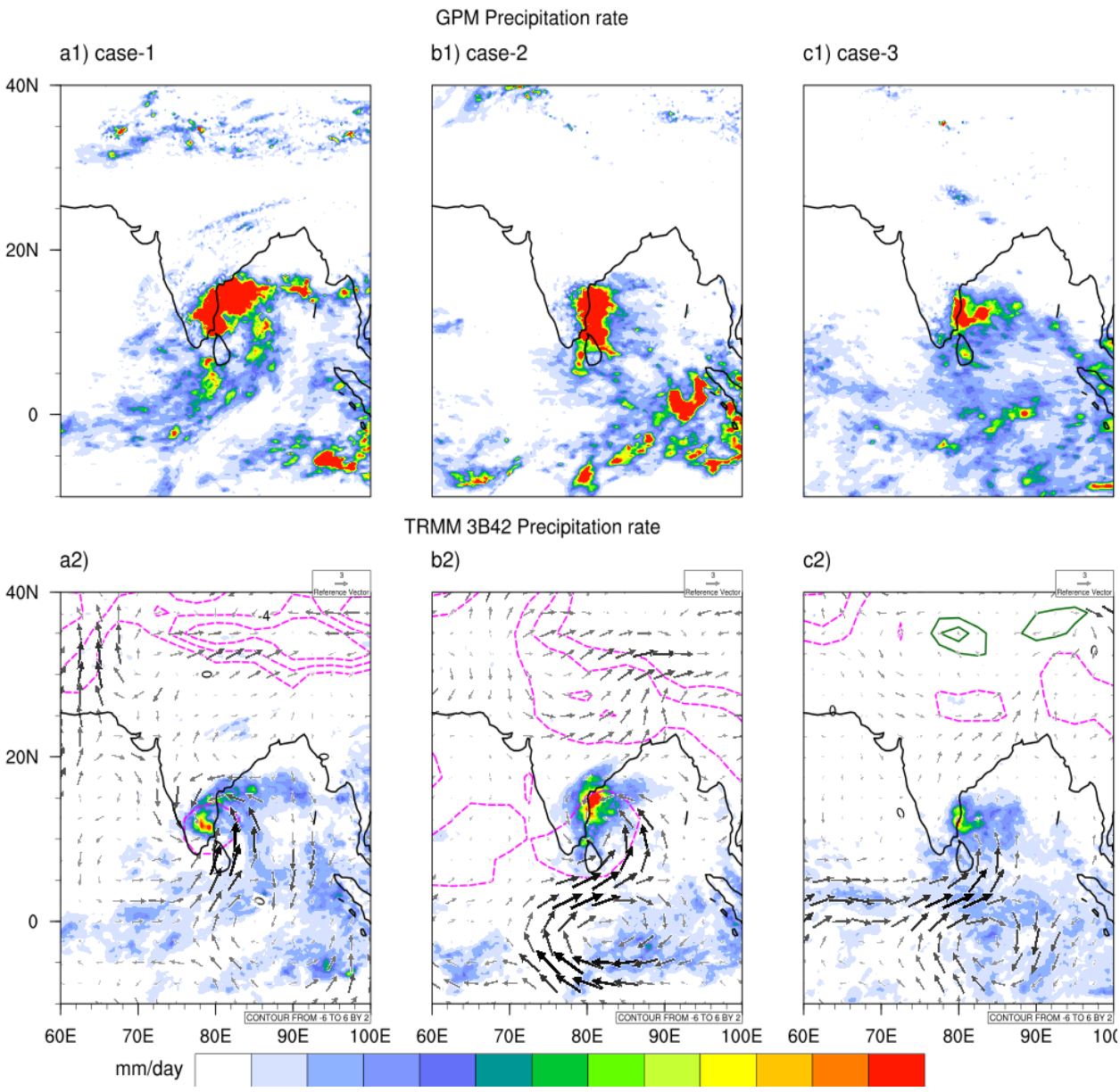

886

887 **Figure 1:** Top row in the panel is composite of GPM precipitation rate (mm/day) and below row in the
888 panel is TRMM 3B42RT precipitation rate during the three cases, i.e., case-1 (left-most column), case-2
889 (middle column), and case-3 (right most column). The dashed contours are NCEP sea level pressure
890 negative anomalies and solid contours are NCEP sea level pressure positive anomalies. Those Vectors
891 represent NCEP wind field anomalies.

892

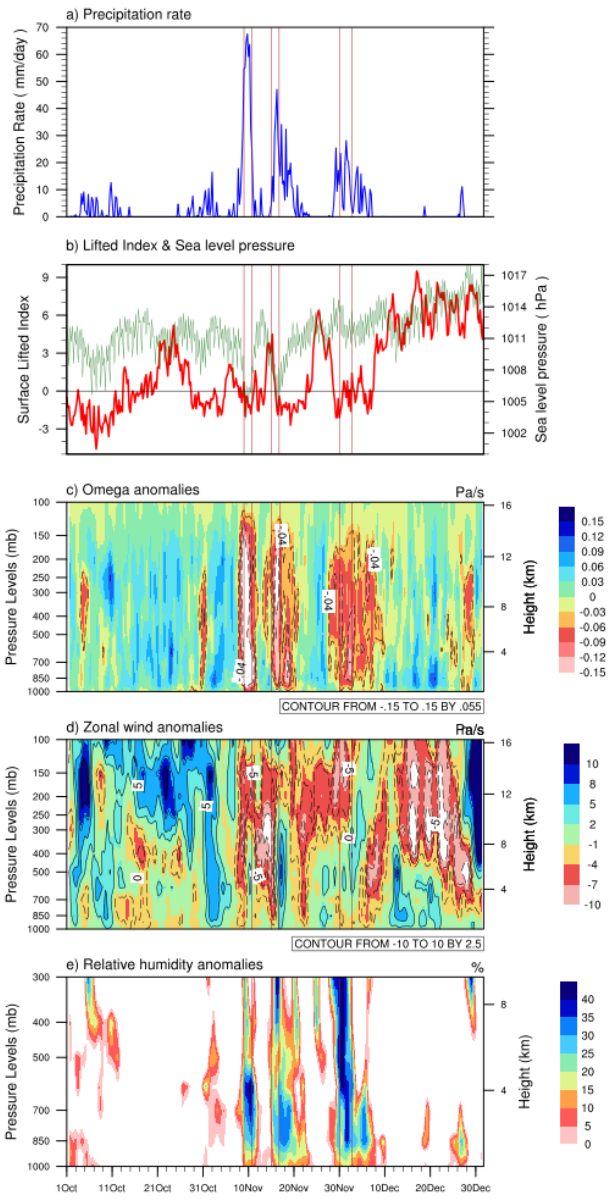

Figure 2: These plots are drawn over latitude 12°N-13°N and longitude 80°E which covers Chennai region of India from October 1 to December 31 of 2015. **a)** NCEP precipitation rate (mm/day) averaged over the mentioned region. b) The red color solid line is NCEP lifted index and green color solid line are NCEP sea level pressure, c) NCEP omega anomalies are, d) NCEP zonal wind anomalies, and e) NCEP relative humidity anomalies. Note NCEP relative humidity is available up to 300 mb. All of these variables were composited for case-1 (Nov 9-Nov 10), case-2 (Nov 15- Nov 16), and case-3 (Nov 30-Dec 2), which were mentioned in black color dashed vertical lines.

901

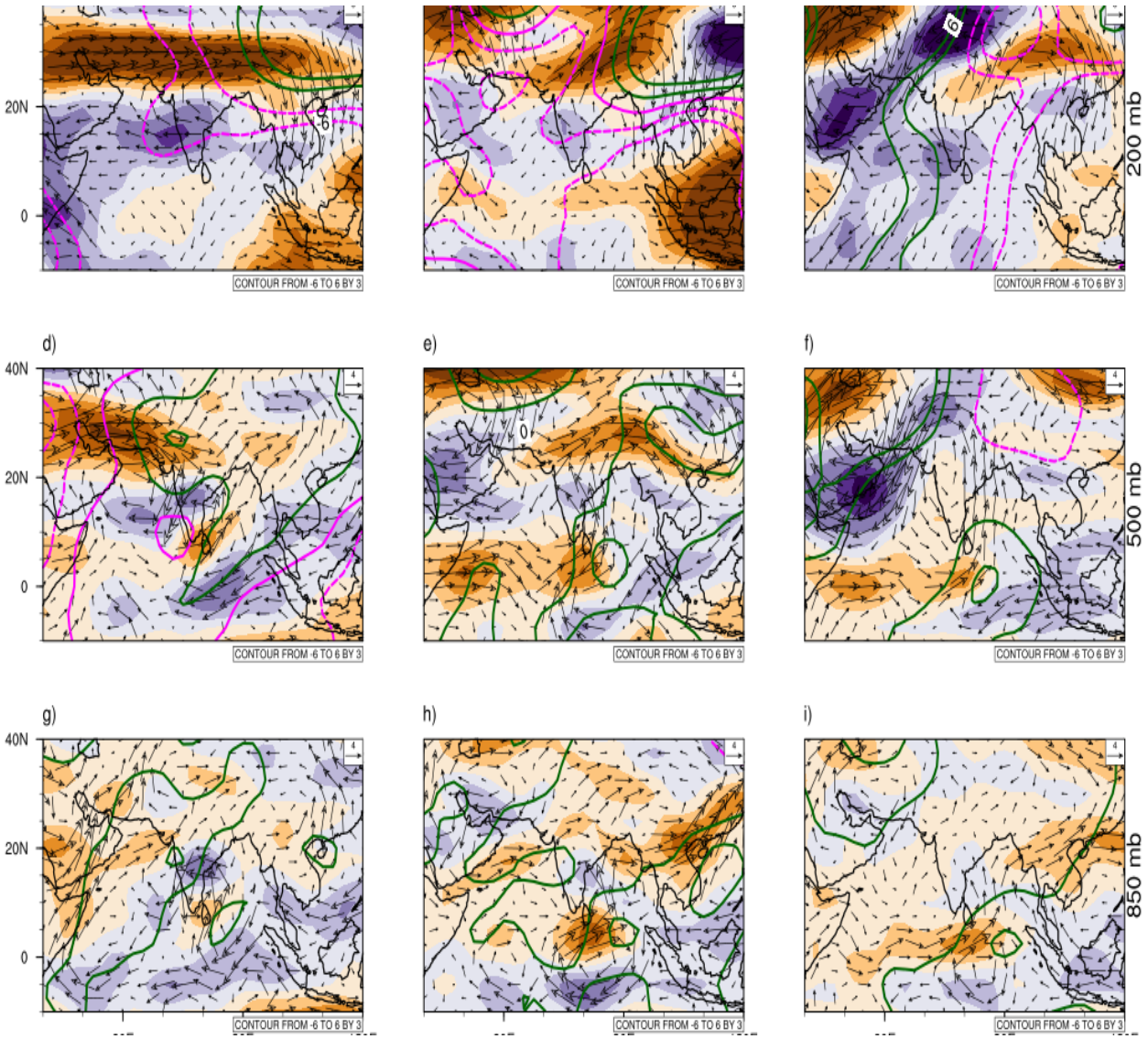

902 **Figure 3:** NCEP zonal wind anomalies composite is created for three cases i.e. (a-d-g) case-1 (Nov 9 to
903 10), b-e-h) case-2 (Nov 15 to 16), and c-f-i) case-3 (Nov 30-Dec 2). Each row of the panel represents a
904 pressure level, which is shown to the right of the last column of the panel. A lowermost row of the panel
905 corresponds to the zonal wind anomalies at 850 mb, and a topmost row of the panel represents 200 mb
906 zonal wind anomalies. Shaded portion is zonal wind anomalies and vectors are anomalous wind. The
907 solid contours are positive velocity potential anomalies, and dashed lines are negative velocity potential
908 anomalies contoured from - 6 to 6 with an interval of three.

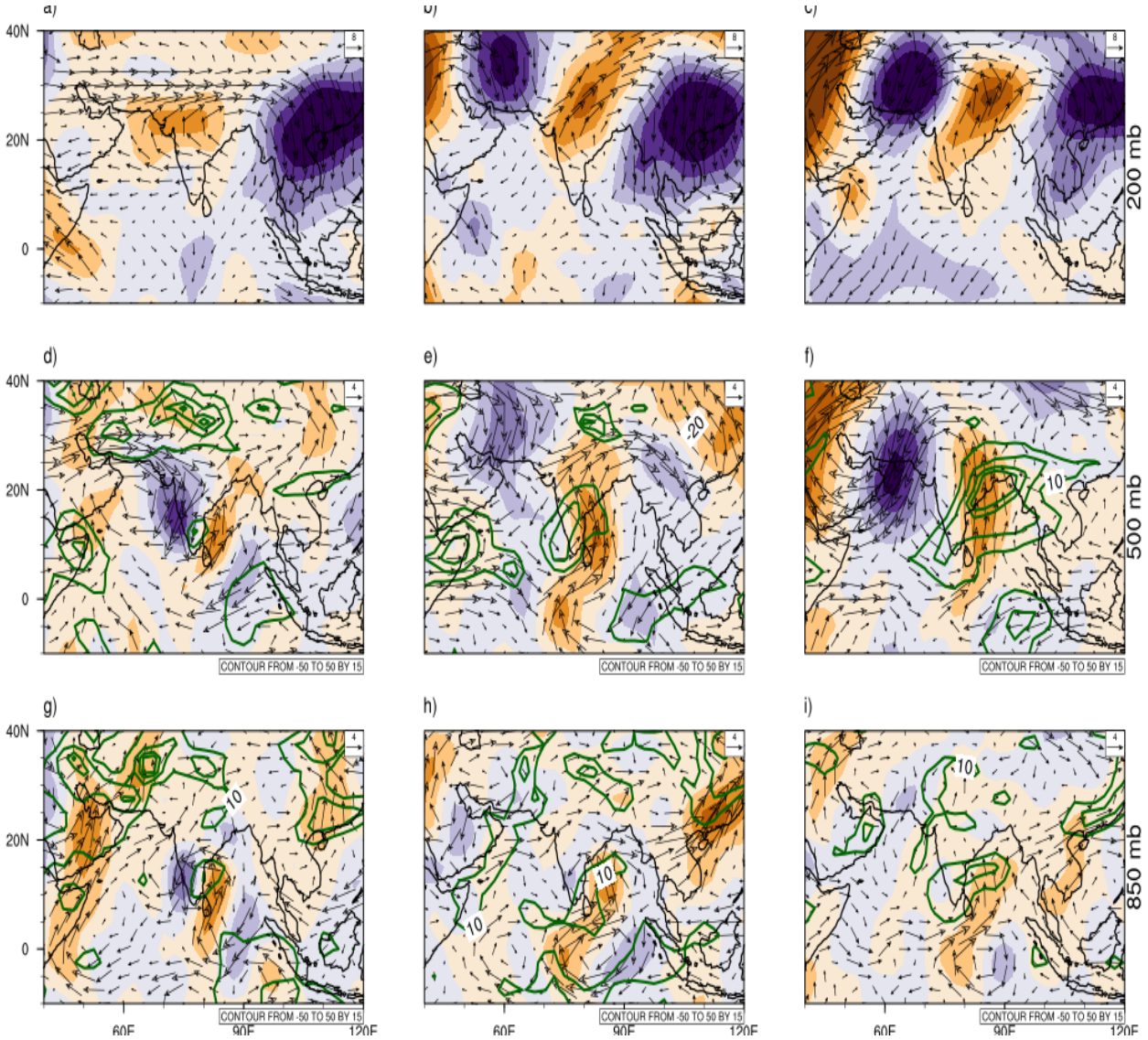

Figure 4: The NCEP meridional wind (m/s) anomalies composite is created for three cases i.e. (a-d-g) case-1 (Nov 9 to 10), b-e-h) case-2 (Nov 15 to 16), and c-f-i) case-3 (Nov 30-Dec 2). Each row of the panel represents a pressure level, which is shown to the right of the last column of the panel. A lowermost row of the panel corresponds to the meridional wind anomalies at 850 mb, and a topmost row of the panel represents 200 mb meridional wind anomalies. Shaded portion is meridional wind anomalies and vectors are anomalous wind. The solid contours are positive relative humidity (%) anomalies contoured from -50 to 50 with an interval of 15. Note NCEP Relative Humidity data is available only up to 300 mb pressure levels.

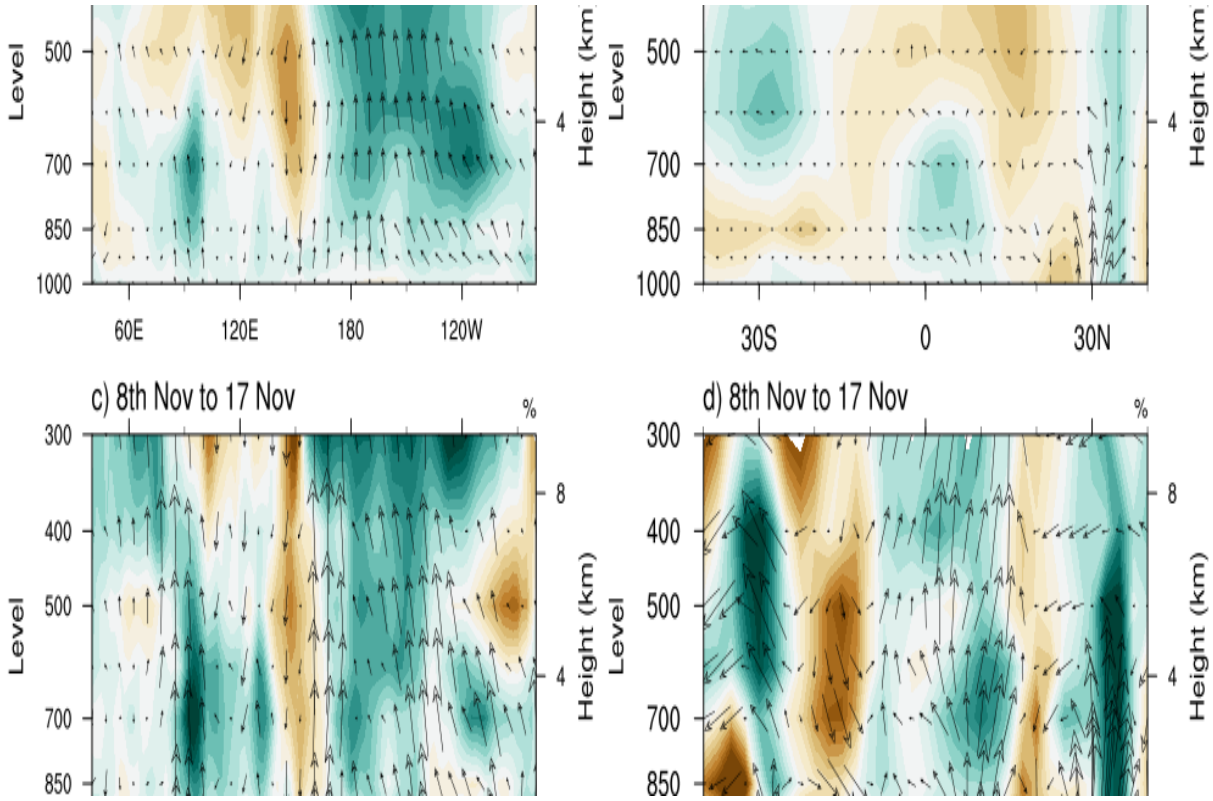

Figure 5: It demonstrates vertical cross-sections of omega, and relative humidity. Left column shows longitudinal cross-section (a, c) and right column (b, d) represents latitudinal cross-sections. Longitudinal cross-sections are averaged over 5°S-5°N, and latitudinal cross-sections are averaged over 75°E-85°E. Top row (a, b) represents OND anomalies, and bottom row shows (c, d) mean of the composite from November 8 to 17, 2015. Here vectors are omega values scaled on the zonal wind for the longitudinal section and meridional for the latitudinal section.

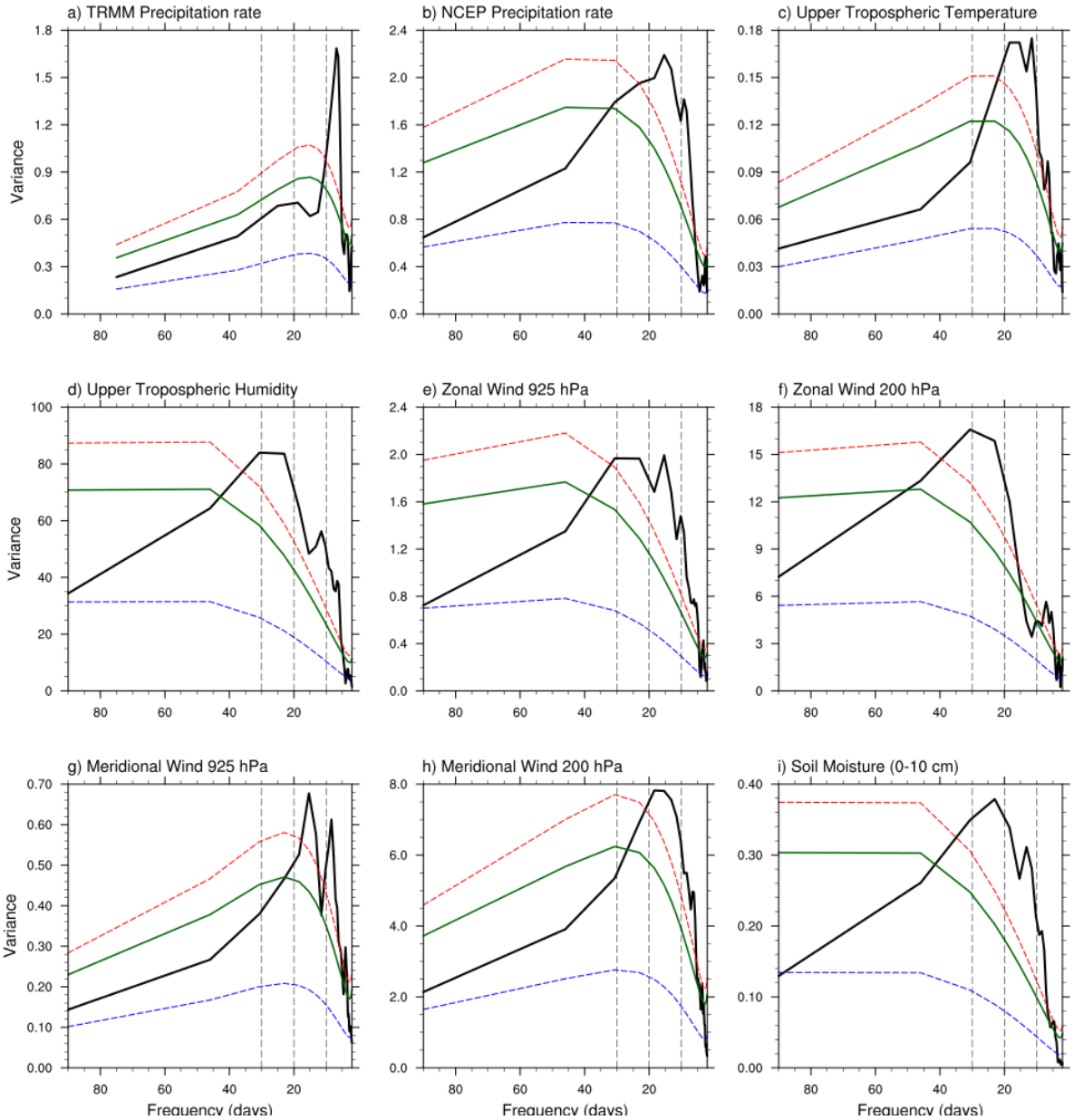

929

930 **Figure 6:** Power spectrum was shown for a) TRMM 3B42 precipitation rate, b) NCEP precipitation rate,
931 c) air temperature, d) zonal wind at 850 mb, e) soil moisture at 0-10 cm and f) Omega at 850 mb, during
932 October-December of 2015 over NEM region (8^{o}N-20^{0}N & 70^{o}E-85^{o}E) is calculated. Green Line shows
933 Markov Red Noise spectrum; red line show upper 95% confidence bounds; and the blue line shows lower
934 5% limits. The x-axis represents periodicity and y-axis represents variance.

935

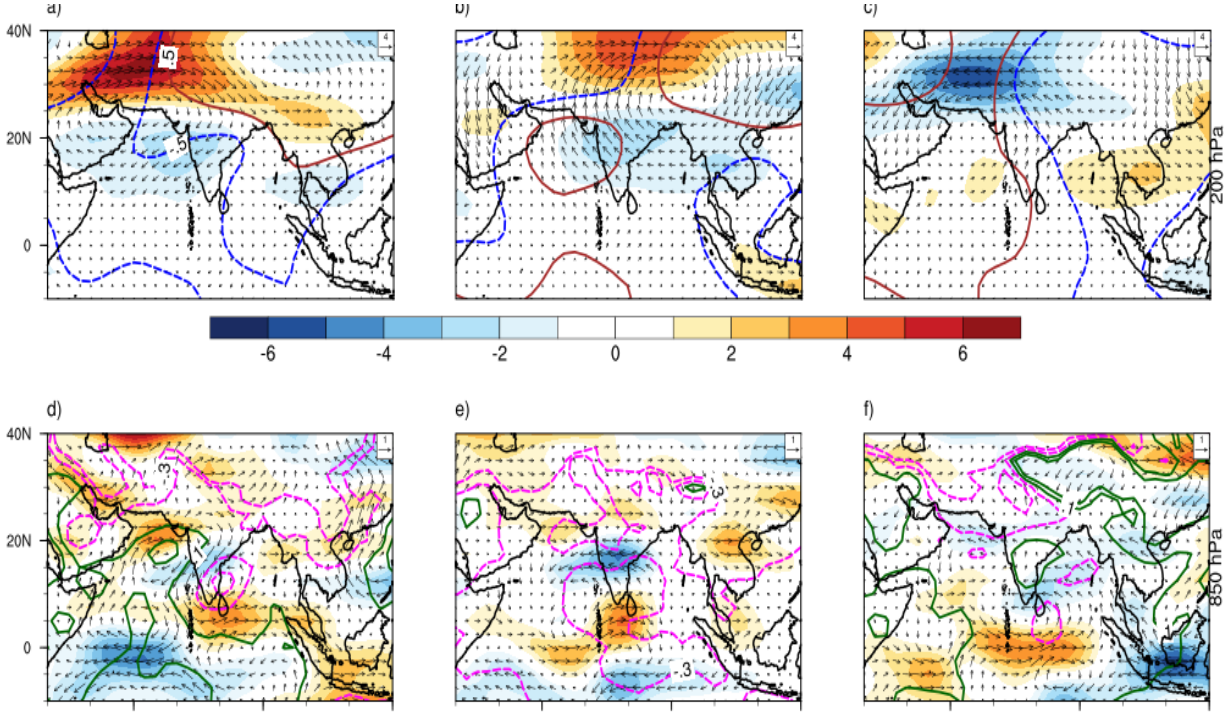

Figure 7: It displays MJO band pass filtered NCEP zonal wind (m/s) anomalies composite is created for three cases i.e. (a-d-g) case-1 (Nov 9 to 10), b-e-h) case-2 (Nov 15 to 16), and c-f-i) case-3 (Nov 30-Dec 2). Each row of the panel represents a pressure level, which is shown to the right of the last column of the panel. A lowermost row of the panel corresponds to the meridional wind anomalies at 850 mb, and a topmost row of the panel represents 200 mb meridional wind anomalies. Shaded portion and vectors are band-pass filtered (30-90 days) zonal wind anomalies. In the bottom panel, the dashed contours are negative sea level pressure (mb) anomalies and solid contours are positive sea level pressure anomalies contoured for -0.3, -0.1, and 0.3. In the topmost panel, the dashed contour is a negative velocity potential anomaly, and the solid line is positive velocity potential anomaly contoured for -4.0, -0.5, 0.5, and 4.0.

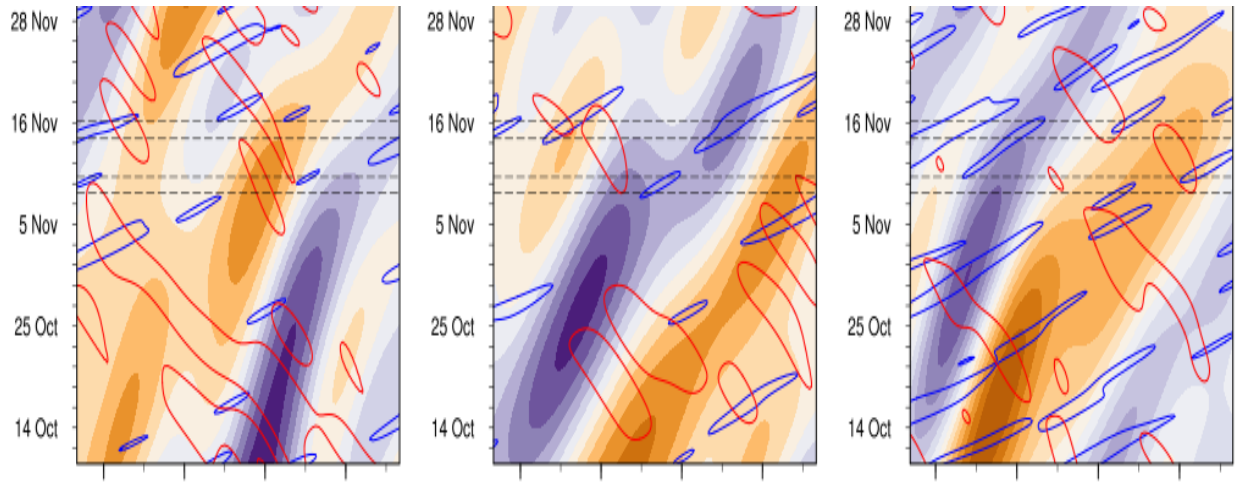

Figure 8: It displays Hovmueller plots of band-pass filtered (30-90 days for MJO, 9-72 days for equatorial Rossby waves, and 2.5-17 days for Kelvin waves) a) zonal wind anomalies at 850 mb (m/s), b) zonal wind anomalies at 200 mb (m/s) and c) NCEP precipitation rate (mm/day). They are averaged over 10°S-10°N. Shaded portion represents MJO filtered waves. Whereas, blue color solid line and red color solid line represent Kelvin waves and equatorial Rossby waves respectively. Dotted black line points the dates during which case-1, case-2, and case-3 happened.

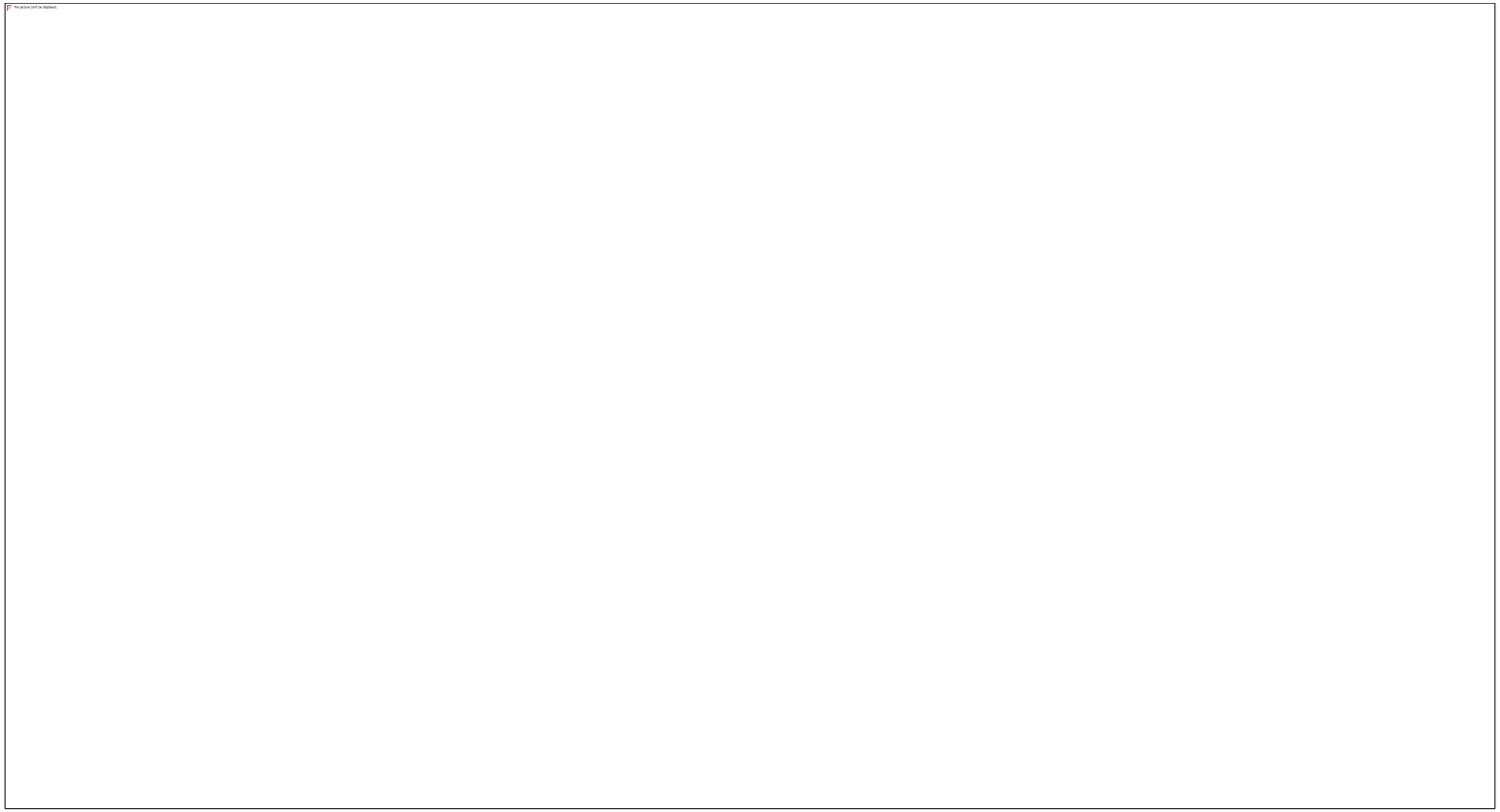

Figure 9: It summarizes the residuals, which are difference between (A) E and N composite (left column), (B) E and M composite, (C) EM blended and N composite, (D) EM blended and M composite, (E) M and N composite, and (F) EM blended and E composite; for NCEP zonal wind anomalies (m/s) and GPCP precipitation rate (mm/day) anomalies. Each row of the panel represents a pressure level, which is shown to the right of the last column of the panel. A lowermost row of the panel corresponds to the wind anomalies at 1000 mb, and precipitation rate anomalies and a topmost row of the panel represents 200 mb zonal wind anomalies. The shaded portions of a second bottom row of the panel to top most rows are zonal wind anomalies. In all of the plots only, more than 95 % significant values are shown (Student's t-test is performed at critical value 0.05).

967

968

969 **Figure 10:** It summarizes the longitudinal vertical cross-sections of omega, and relative humidity
970 anomalies of A, B, C, D, E, and F residuals, which are differences of E & N, E & M, EM & N, EM &
971 M, M & N and EM & E composites, and these composites were explicitly discussed in section 3.6.
972 These longitudinal cross-sections were averaged over 5^{o}S-5^{o}N. Here vectors are omega values scaled w.r.t
973 to the zonal wind, and colored region shows relative humidity anomalies.

974

975

976 **Figure 11**: It describes the latitudinal vertical cross-sections of omega, and relative humidity anomalies of
977 A, B, C, D, E, and F residuals, which are differences of E & N, E & M, EM & N, EM & M, M & N,
978 and EM & E composites, and these composites are apparently discussed in section 3.6. These
979 latitudinal cross-sections were averaged over 75^{o}E-85^{o}E. Here vectors are omega values scaled w.r.t to the
980 meridional wind, and colored area shows relative humidity anomalies.

981

982

983

984

985

986

Figure 12: It demonstrates the response of GPCP precipitation anomalies to NCEP zonal wind anomalies in MJO (red; M), Normal (green; N), El Nino (blue; E) and El Nino & MJO mixed wave (magenta; EM) composites. Here composites are done for a period 1997-2014 in OND season. The black color markers represent the residuals A, B, C, D, E, and F; these residuals are interactions of M & N, E & N, E & M, EM & N, EM & M and EM & E composites respectively. The precipitation anomalies shown above are area averaged over 8^{o}N-16^{o}N & 75^{o}E-84^{o}E, and zonal wind anomalies are area averaged over 0^{o}-6^{o}N & 70^{o}E-80^{o}E for MJO and 2^{o}S-4^{o}N & 90^{o}E- 98^{o}E for El Nino composites. The statistical characteristics like p-value (p), correlation coefficient (r), and standard deviations (std) of each composite are also shown in the figure.